Accepted Manuscript

Iron cycling and stable Fe isotope fractionation in Antarctic shelf sediments, King George Island

Susann Henkel, Sabine Kasten, Jan Hartmann, Adrián Silva Busso, Michael Staubwasser

Please cite this article as: Henkel, S., Kasten, S., Hartmann, J., Silva Busso, A., Staubwasser, M., Iron cycling and stable Fe isotope fractionation in Antarctic shelf sediments, King George Island, *Geochimica et Cosmochimica Acta* (2018), doi: https://doi.org/10.1016/j.gca.2018.06.042

Iron cycling and stable Fe isotope fractionation in Antarctic shelf sediments, King George Island

Susann Henkel[1,2], Sabine Kasten[1,2,3], Jan Hartmann[4], Adrián Silva Busso[5], Michael Staubwasser[6]

[1] Alfred Wegener Institute Helmholtz Centre for Polar and Marine Research, Am Handelshafen 12, 27570 Bremerhaven, Germany

[2] MARUM – Center for Marine Environmental Sciences, University of Bremen, Leobener Str. 8, 28359 Bremen

[3] University of Bremen, Faculty of Geosciences, Klagenfurter Strasse, 28359 Bremen, Germany

[4] Institut für Geowissenschaften, Universität Heidelberg, Im Neuenheimer Feld 236, 69120 Heidelberg, Germany

[5] Instituto Nacional del Agua, Empalme J. Newbery km 1, 620, Ezeiza, Buenos Aires, Argentina

[6] University of Cologne, Zülpicher Str. 49a, 50674 Cologne, Germany

Corresponding author: Susann Henkel (susann.henkel@awi.de)

Abstract

Iron (Fe) fluxes from reducing sediments and subglacial environments are potential sources of bioavailable Fe into the Southern Ocean. Stable Fe isotopes (δ^{56}Fe) are considered a proxy for Fe sources and reaction pathways, but respective data are scarce and Fe cycling in complex natural environments is not understood sufficiently to constrain respective δ^{56}Fe "endmembers" for different types of sediments, environmental conditions, and biogeochemical processes.

We present δ^{56}Fe data from pore waters and sequentially extracted sedimentary Fe phases of two contrasting sites in Potter Cove (King George Island, Antarctic Peninsula), a bay that is affected by fast glacier retreat. Sediments close to the glacier front contain more easily reducible

Fe oxides and pyrite and show a broader ferruginous zone, compared to sediments close to the ice-free coast, where surficial oxic meltwater streams discharge into the bay. Pyrite in sediments close to the glacier front predominantly derives from eroded bedrock. For the high amount of easily reducible Fe oxides proximal to the glacier we suggest mainly subglacial sources, where Fe liberation from comminuted material beneath the glacier is coupled to biogeochemical weathering processes (likely pyrite oxidation or dissimilatory iron reduction, DIR). Our strongest argument for a subglacial source of the highly reactive Fe pool in sediments close to the glacier front is its predominantly negative δ^{56}Fe signature that remains constant over the whole ferruginous zone. This implies *in situ* DIR does not significantly alter the stable Fe isotope composition of the accumulated Fe oxides. The nonetheless overall light δ^{56}Fe signature of easily reducible Fe oxides suggests pre-depositional microbial cycling as it occurs in potentially anoxic subglacial environments. The strongest ^{56}Fe-depletion in pore water and most reactive Fe oxides was observed in sediments influenced by oxic meltwater discharge. The respective site showed a condensed redox zonation and a pore water δ^{56}Fe profile typical for *in-situ* Fe cycling.

We demonstrate that the potential of pore water δ^{56}Fe as a proxy for benthic Fe fluxes is not straight-forward due to its large variability in marine shelf sediments at small spatial scales (-2.4‰ at the site proximal to oxic meltwater discharge vs. -0.9‰ at the site proximal to the marine glacier terminus, both at 2 cm sediment depth). The controlling factors are multifold and include the amount and reactivity of reducible Fe oxides and organic matter, the isotopic composition of the primary and secondary ferric substrates, sedimentation rates, and physical reworking (bioturbation, ice scraping). The application of δ^{56}Fe geochemistry may prove valuable in investigating biogeochemical weathering and Fe cycling in subglacial environments. This requires, however (similarly to the use of δ^{56}Fe for the quantification of benthic fluxes), that the spatial and temporal variability the isotopic endmember is known and accounted for. Since geochemical data from subglacial environments is very limited, further studies are needed in order to sufficiently

assess Fe cycling and fractionation at glacier beds and the composition of discharges from those areas.

1   Introduction

Global warming is leading to considerable glacier retreat in the Arctic and in West Antarctica resulting in enhanced iron fluxes into coastal and ocean regions such as the Southern Ocean (SO), where phytoplankton growth is otherwise Fe-limited (e.g., Boyd 2002, Cook et al. 2005, Raiswell et al. 2008, Death et al. 2014). Primary productivity in such high-nutrient-low-chlorophyll (HNLC) ocean areas can be stimulated by Fe fertilization resulting in a higher uptake of atmospheric CO_2 and enhanced burial of organic matter ("biological carbon pump"). This effect represents a negative feedback to climate change (e.g., Martin 1990, Raiswell et al. 2008), but is hard to quantify since Fe fluxes from Antarctica are currently not well constrained. According to Raiswell et al. (2016) icebergs deliver between 3.2 and 25 Gmol a^{-1} (180 – 1400 Gg a^{-1}) of bioavailable Fe into the SO, whereas aeolian transport accounts for an input of only <0.03 Gmol a^{-1} (<1.7 Gg a^{-1}). Benthic fluxes from shelf sediments may deliver up to 790 Gg a^{-1} of bioavailable Fe (Monien et al. 2014). The significance of this source is also indicated by increasing dissolved Fe concentrations in the water column from surface water towards the sediment surface and generally decreasing dissolved Fe concentrations with increasing distance from the continental shelves in the Atlantic sector of the SO (De Jong et al. 2012). Subglacial meltwater has been estimated to contribute between 8.9 and 11000 Gg Fe a^{-1} assuming fully anoxic meltwater release, but only 0.03 to 5.9 Gg a^{-1} when taking precipitation in oxic shelf waters into account (Wadham et al. 2013). Despite the increasing number of studies related to Fe fluxes in polar regions, all estimates show large uncertainties reflecting logistical and methodological constraints with respect to the inaccessibility of specific areas (e.g., subglacial meltwater) and the difficulties concerning trace-metal clean sampling in such remote areas.

Stable iron isotope signatures (δ^{56}Fe, δ^{57}Fe) may develop into a useful tool to discriminate different Fe sources and transport and reaction pathways (e.g., Rouxel and Auro 2010, John et al. 2012, Conway and John 2014). In polar regions, where the impact of Fe cycling on the regulation of plankton growth is high (e.g., Dierssen et al. 2002, Statham et al. 2008) and where uncertainties with respect to Fe fluxes are large, the application of Fe isotope geochemistry seems particularly promising.

Microbial redox cycling is known to go along with a strong Fe isotope fractionation (e.g., Beard and Johnson 2004). Since anoxic shelf sediments as well as glacier beds are habitats for a variety of microbes including Fe reducers (e.g., Lovley 1991, Nixon et al. 2017), these environments produce solid and dissolved Fe with δ^{56}Fe signatures that are distinct from Fe mobilized solely by physical weathering (e.g., Fantle and DePaolo 2004). In (sub)glacial environments, the isotopic signature of Fe minerals may be modified, e.g., by extensive pyrite oxidation or dissimilatory iron reduction (DIR) before Fe is delivered into shelf waters and sediments (Milucki et al. 2009, Stevenson et al. 2017). After their deposition, all reactive Fe phases, deriving from both, physical and biogeochemical weathering, may again be isotopically modified during early diagenesis.

Compared to subglacial Fe cycling, isotope fractionation in shallow marine sediments is reasonably well understood: DIR produces isotopically light dissolved Fe (down to -3‰, Johnson and Beard 2005, Severmann et al. 2006, Henkel et al. 2016) compared to the average isotopic composition of terrestrial igneous rock (δ^{56}Fe = ~0.09±0.05‰, Beard et al. 2003). The ongoing preferential liberation of [54]Fe typically causes a trend towards higher Fe isotope values of the residual Fe oxide fraction with depth. However, to our knowledge this is the first study investigating Fe isotope fractionation by early diagenetic processes in a glaciated marine area.

We investigate Fe cycling in combination with phase-specific δ^{56}Fe signatures in shallow marine sediments from Potter Cove, a bay of King George Island (West Antarctic Peninsula) that is strongly affected by glacier retreat (Rückamp et al. 2010, 2011). This study aims to assess differences in the δ^{56}Fe composition of shelf sediments that are dominated by input from a tidewater vs. a land-

terminating draining glacier of the polythermal Fourcade Glacier system with distinct mechanisms of Fe delivery (subglacial vs. surficial oxic meltwater discharge). If signals of subglacial weathering can be detected in the marine sediment, this would be an important step towards a source fingerprinting that may enable a better estimation of subglacial Fe fluxes. In addition, the assessment of the variability of the Fe isotopic composition of solid and dissolved phases in marine shelf sediments may also be useful to evaluate the potential of δ^{56}Fe as a proxy for benthic fluxes (Staubwasser et al. 2006, Homoky et al. 2009). We hypothesize that the degree of *in situ* Fe isotope fractionation in pore water and the sedimentary reactive Fe phases depends on the degree of DIR and sulfate reduction and, thus, the respective environmental control parameters such as the availability of organic matter and reducible Fe oxides.

We examine pore waters and the solid phase of short sediment cores from Potter Cove. We sequentially extracted reactive Fe mineral phases and processed the extracts for the subsequent analysis of δ^{56}Fe according to the procedure developed by Henkel et al. (2016). Our objectives were to determine (1) if and how glacier melt affects the composition of sediments in terms of Fe reactivity, (2) whether the Fe isotopic composition of reactive Fe in the sediments is indicative of distinct Fe sources, and (3) how geochemical conditions and biogeochemical processes in the sediment affect pore water and sedimentary δ^{56}Fe signatures.

2   Regional setting and geochemical background

King George Island (KGI, also Isla 25 de Mayo) is located at the northern tip of the West Antarctic Peninsula (WAP). With 1250 km² it is the largest of the South Shetland Islands. The working area, Maxwell Bay, is located between 62°10' and 62°20′S and 58°35′and 59°00′W (Fig. 1). Several tributary fjords are adjoined to Maxwell Bay: Collins Harbour in the North, Marian Cove in the East and Potter Cove, the main study area, in the Southeast. Potter Cove is about 4 km long, 2.5 km wide and separated into an inner and an outer cove by a 30 m deep submarine sill (Klöser et al. 1994,

Wölfl et al. 2014). Water depths are up to 50 m in the inner and up to 200 m in the outer cove (Klöser et al. 1994). The Fourcade Glacier is a polythermal glacier (Falk et al. 2018) draining into Potter Cove. It covered half of the inner cove until the 1950's. Since then, the tidewater front retreated by more than 1 km (Rückamp et al. 2011). At present, the northeastern part of Potter Cove is characterized by the tidewater draining glacier, whereas the southern part (Potter Peninsula) is characterized by a net of surficial meltwater streams (Fig. S1).

The water circulation in Potter Cove is mainly driven by a bidirectional (E-W) wind field (Klöser et al. 1994, Roese and Drabble 1998). The average tidal range in Potter Cove is 1.5 m (Schöne et al. 1998) causing currents of subordinate intensity. Klöser et al. (1994) and Roese and Drabble (1998) described a cyclonic gyre as long-term current pattern, which causes the entrance of cold and saline water from Maxwell Bay into the northwestern part and outflow in the southern part of Potter Cove. During its clockwise flow in the bay seawater mixes with sediment-laden meltwater, i.e. from surficial meltwater streams at the southern coast (Figs. 1, S2). Outflow is inhibited with increasing west winds, causing a build-up of a brownish plume in the bay (Klöser et al. 1994). The water column is oxic year-round.

The rocks outcropping on Potter Peninsula, the area south of Potter Cove, are of volcanic origin and belong to the KGI Supergroup (Kraus and del Valle 2008). A prominent feature of Potter Peninsula is the Three Brothers Hill, an andesitic plug that remained from an Eocene stratovolcano. Rocks prevalent on Potter Peninsula are pyroclastica, basaltic, and andesitic lava flows as well as hypabyssal intrusions, sills, and dykes. Rocks of KGI, in particular of Barton Peninsula north of Potter Cove, have been described to contain "quartz-pyrite lodes" of hydrothermal origin (Ferguson 1921, Littlefair 1978, So et al. 1995) and have been shown to undergo sulfide oxidation: In Marian Cove (Fig. 1), the neighboring bay of Potter Cove to the North, Dold et al. (2013) detected acid rock drainage (caused by pyrite oxidation at the glacier bed) and a related accumulation of significant amounts of Fe (oxyhydr)oxides and oxyhydride sulfates at the beach. The discharging groundwater had a pH of 3.2 and high dissolved Fe concentrations (465 µM, mostly Fe^{2+}). Subglacial meltwater is

common in Antarctica. It provides suitable conditions for microbial life at glacier beds, which drives biogeochemical cycles and affects downstream environments into which the water is discharged (Mikucki et al. 2016). Meltwater affected by biogeochemical weathering beneath glaciers may drain superficially, but can also percolate into sediments and rocks beneath the glacier forming a subterranean Fe^{2+} plume entering the bay as groundwater (Dold et al. 2013).

About 80% of the seafloor in Potter Cove is covered by soft sediment, mostly silt and sandy silt. There are strong spatial differences in the thickness of the sediment cover depending on morphology and bed shear stresses. Fine-grained sediments prevail in the inner cove and at deeper depth in the outer cove. They originate from the Fourcade Glacier and meltwater streams. Hard ground has been found especially in the northwestern part of the outer cove, where wave-induced erosion of fine material is high (Wölfl et al. 2014). Total organic carbon (TOC) contents in surface sediments are low (<0.5 wt%) in the newly ice-free area in the eastern part and highest (~1.2 wt%) in deep troughs in the center of Potter Cove (Fig. 7 in Monien et al. 2014).

3 Methods

3.1 Pore water and sediment sampling

Pore water and sediment of Potter Cove and Maxwell Bay were collected during the Antarctic summers 2012 and 2013 and processed and analyzed in the Dallmann Laboratory (AWI) of the Argentine Research Base Carlini (Fig. 1). Short sediment cores were gained from a rubber boat either by deployment of an Uwitec corer or by divers that pushed liners into the ground (Table S1). The pore water was sampled with rhizons (Seeberg-Elverfeldt et al. 2005) immediately after lifting the cores on board in order to avoid disturbances during the partly rough return to the Dallmann Laboratory. For each sampling point, one core was dedicated to pore water analyses (SO_4^{2-}, Fe^{2+}, alkalinity, NH_4^+) and a second core was transported back to the Dallmann Laboratory for sediment sampling. Sediment samples were taken within a few hours after core retrieval using cut-off syringes. Those were sealed and kept at -20°C under Ar until processing. At station STA04 (11 m water depth)

and STA10 (20 m water depth), additional cores were taken for pore water stable Fe isotope ($\delta^{56}Fe_{pw}$) sampling. The sampling of separate cores at each station potentially resulted in slight offsets between the respective geochemical profiles.

3.2   Pore water analyses

Fe^{2+} was analyzed using the ferrozine method (Stookey 1970) in the Dallmann Laboratory (detection limit: 0.2 μM, quantification limit: 0.4 μM). Alkalinity was measured by titration with HCl (2012 campaign) and spectrophotometrically after Sarazin et al. (1999) using a Multiskan microplate reader (2013 campaign). Alkalinity data produced for one core using both methods resulted in identical profiles (Fig. S3), so results from both campaigns are comparable. Ammonium (NH_4^+) was determined conductometrically (in 2012) and spectrophotometrically using a microplate reader (in 2013) a few hours after sampling. Sulfate samples (1:50 dilutions with ultrapure water) were analyzed by ion chromatography (Metrohm IC Net 2.3) at the Alfred Wegener Institute, Helmholtz Centre for Polar and Marine Research (AWI).

Pore water was acidified with double distilled HCl and stored at 4°C until processing for $\delta^{56}Fe$ analysis at the University of Cologne. The required mass inventory for pore water $\delta^{56}Fe$ ($\delta^{56}Fe_{pw}$) processing and analysis was ~1 μg. Samples were adjusted to pH 2 with NH_4OH s.p., H_2O_2 was added to a concentration of 10 μM to oxidize Fe^{2+} to Fe^{3+}, and iron was subsequently pre-concentrated and extracted from the salt matrix by column chromatography (NTA Superflow columns, Qiagen) (Lohan et al. 2005). Samples were further purified by column separation using Dowex® 1X8 resin. Afterwards, concentrations were matched to 0.2 ppm for isotope analysis on a ThermoFinnigan Neptune Multicollector-ICP-MS at the Steinmann Institute (Bonn). The Neptune was equipped with an ESI Apex-Q desolvator and we applied the standard-sample bracketing method using the IRMM-014 standard (e.g., Schoenberg and von Blanckenburg 2005). Data are reported as

$$\delta^{56}Fe \ [‰] = (^{56}Fe/^{54}Fe_{sample})/(^{56}Fe/^{54}Fe_{IRMM-014}) - 1] * 1000.$$

The external precision of the analyses was monitored with the inhouse standard JM (Johnson & Matthey Fe Puratronic wire). The measured JM values were $0.46 \pm 0.11‰$ (error is 1SD, target value $0.42 \pm 0.05‰$, Schoenberg and von Blankenburg 2005). Duplicate sample measurements (Fig. 4f) were identical within analytical uncertainty. Uncertainty for individual samples as indicated by error bars in Fig. 4 is 1SD of 20 consecutive measurements belonging to one analysis.

3.3   Solid phase analyses

We used ~50 mg of freeze-dried and ground sediment for total acid digestion (3 mL HCl + 2 mL HNO_3 + 0.5 mL HF) in a CEM Mars Xpress microwave system at AWI. Elemental contents were determined by ICP-OES analysis (Iris Intrepid II) of the dissolved sediment. Recoveries for a total of nine processed sediment standards (NIST SRM 2702) were $94.4 \pm 1.5\%$ for Al, $101.8 \pm 0.6\%$ for Fe (Fe_{total}), $96.0 \pm 0.7\%$ for Mn, and $106.0 \pm 1.2\%$ for S.

Acid volatile sulfur (AVS) and chromium reducible sulfur (CRS) were determined gravimetrically with a two-step extraction of ~1 g of dry sediment. (Abbreviations of these and all following parameters are listed in Table 1.) Sample splits for these extractions were taken from anoxically stored sediment a few days before analysis. AVS was reduced using 6M HCl (Cornwell and Morse 1987) and CRS with a $CrCl_2$ solution (e.g., Zhabina and Volkov 1978, Canfield et al. 1986). The liberated H_2S was trapped as Ag_2S. Fe monosulfide and pyrite contents were then calculated from extracted sulfur using the stoichiometry 1:1 (FeS) and 1:2 (FeS_2), respectively. Repetitive analyses of an inhouse standard (anoxic sediment from the North Sea) resulted in FeS and pyrite contents of 0.08 ± 0.06 wt% (n = 28) and 0.96 ± 0.09 wt% (n = 26), respectively.

Sequential extractions were performed after Poulton and Canfield (2005) and Henkel et al. (2016) using ~50 mg of dry sediment and 5 mL of a) Na-acetate for Fe-carbonates and surface-reduced Fe(II) (Fe_{aca}), b) hydroxylamine-HCl for easily reducible Fe-oxides (ferrihydrite, lepidocrocite) (Fe_{hyam}), c) Na-dithionite/citrate for reducible Fe-oxides (mostly goethite and hematite and some

magnetite) (Fe$_{di-ct}$), and d) ammonium oxalate/oxalic acid for magnetite (Fe$_{oxa}$). The procedures for matrix removal of the extracts and δ^{56}Fe analyses by MC-ICP-MS are described in detail in Henkel et al. (2016). The JM standard was measured every six samples. Only isotope values produced in between JM standards that matched the target value 0.42 ± 0.05‰ (see above) were considered in the data evaluation. Certipur® standards that underwent the same chemical processing as all samples are isotopically identical within error to the unprocessed solution (δ^{56}Fe = 0.15 ± 0.03‰, n = 9) as given in Henkel et al. (2016): 0.14 ± 0.03‰ for acetate (n = 7), 0.13 ± 0.02‰ for hydroxylamine–HCl (n = 5), 0.09 ± 0.03‰ for dithionite–citrate (n = 7), and 0.14 ± 0.04‰ for oxalate (n = 5). In addition, a hematite–goethite standard with a known isotopic composition (0.26 ± 0.03‰, n = 11, Staubwasser et al. 2006) was leached with dithionite and processed, which resulted in a δ^{56}Fe value of 0.30 ± 0.07‰ (n = 5).

4   Results

4.1   Spatial differences in early diagenetic conditions in Potter Cove and Maxwell Bay

We classified all sampled sites into three groups according to the main feature that potentially determines their depositional characteristics: (I) Stations proximal to the discharge of surficial oxic meltwater streams that derive from the glacier edge and pass some hundreds of meters over ice-free, rocky area before reaching Potter Cove (STA04, STA11), (II) stations in the central area of the bay or proximal to the coast, but not directly influenced by surficial meltwater runoff (STA 03, STA05, STA06, STA14, STA15, STA16, STA17), and (III) stations that are located proximal to the glacier terminus, where the glacier is marine-terminating (STA01, STA08, STA09, STA10, STA13) (Fig. 2). We then tried to identify trends or differences between the groups with respect to the degree of their early diagenetic alteration.

Sediments proximal to oxic surficial meltwater streams that drain ice-free parts of Potter Peninsula (Group I), are characterized by a comparatively narrow ferruginous zone, a blackish

sediment color and sulfide smell at shallow depth. Those sediments appeared strongly bioturbated and show a significant sulfate decrease and alkalinity and ammonium increases with depth (Fig. 3a). Sediments in troughs in the central Potter Cove as well as those proximal to ice-free areas of Ardley Island and Fildes Peninsula (STA05, STA06) (Group II) show more extended ferruginous zones down to ~20 cm depth and higher Fe^{2+} concentrations (mostly up to 200 µM, up to 850 µM at STA06) compared to the sites of Group I (up to 110 µM) (Fig. 3b). The pattern, however, is not straightforward. Neighboring stations partly show very different geochemical profiles, e.g., STA03 (45 m WD, narrow ferruginous zone, sulfate decrease with depth) and STA16 (37 m WD, broad ferruginous zone, no significant sulfate decrease). The ferruginous zones at stations proximal to the glacier fronts in the northern and eastern part of Potter Cove (STA01, STA10, STA13), Marian Cove (STA09), and Collins Harbour (STA08) (Group III) reach down to >25 cm sediment depth and sulfate decrease as well as alkalinity and ammonium increases are less apparent (Fig. 3c).

4.2   Reactive Fe and related isotope fractionation in sediments

For detailed studies of the phase-specific stable Fe isotope fractionation we chose two contrasting stations, one from the surficial oxic meltwater-dominated southern part of Potter Cove showing a linear decrease in sulfate concentrations with depth (STA04), and one with a broad ferruginous zone proximal to the glacier front in the northern part of Potter Cove (STA10).

Fe_{total} contents are similar at both stations and amount to ~6 wt% (Fig. 4, Table S2). Reactive Fe (Fe_{react}), here defined as the sum of sequentially extracted Fe (Fe_{aca} + Fe_{hyam} + Fe_{di-ct} + Fe_{oxa}), constitutes about a third of Fe_{total} (Fig. 4b, e). We exclude sulfide-Fe from the Fe_{react} fraction as we focus on Fe species that are reactive in terms of DIR. Fe_{di-ct} (~40 - 50% of Fe_{react}) and Fe_{oxa} (30 - 40% of Fe_{react}) are the dominant reactive Fe fractions. Fe_{aca} and Fe_{hyam} amount to 2 - 3% and 10 - 18% of Fe_{react}, respectively.

Sediments at the southern station STA04 contain significantly lower amounts of easily reducible oxides (Fe_{hyam}) compared to those close to the glacier front at STA10 (0.18 ± 0.03 wt% and 0.28 ± 0.03 wt%, respectively; variation is 1SD; Fig. 4a, d and Table S2). Fe_{hyam} contents show a slight decrease with depth at both stations, but the trend disappears when contents are normalized to Fe_{react} (Fig. 5a, c). All other extracted Fe phases (Fe_{aca}, Fe_{di-ct} and Fe_{oxa}) are present at comparable or higher contents at STA04 compared to STA10 (Table S2): Fe_{aca} comprises 0.8 to 4.8% of Fe_{react} at STA04 and 1.0 to 3.7% at STA10, Fe_{hyam} 4.5 to 10.8% (STA04) and 13.2 to 18.4% (STA10), Fe_{di-ct} 47.3 to 58.7% (STA04) and 38.5 to 52.4% (STA10), and Fe_{oxa} 26.8 to 43.8% (STA04) and 32.4% to 43.0% (STA10).

Mn/Al and, to a lesser extent, Fe_{react}/Fe_{total} decrease from core top to about 2 cm depth at STA04 (Fig. 4b). There is a slight overall decrease in Fe_{react}/Fe_{total} with depth at STA10. Dissolved Fe^{2+} reaches its maximum of 112 µM at 4 cm at STA04 (Fig. 4c) and 96 µM at 10 cm depth at STA10 (Fig. 4f). The fraction of Fe bound in pyrite is lower at STA04 (<0.1 wt% Fe_{pyrite}, Fig. 5b) compared to STA10 (up to 0.2 wt% Fe_{pyrite}, Fig. 5d), which is also reflected by significantly lower S/Al ratios at STA04 (Fig. 4b, e). Fe bound in AVS (Fe_{AVS}) is <0.05 wt% at both stations (Fig. 5b, d). The uppermost 2 cm of the sediment column are AVS-free.

Pore water Fe^{2+} is isotopically light ($\delta^{56}Fe_{pw} < 0$‰) at both stations over the whole core length (Fig. 4c, f). The ^{56}Fe-depletion, especially towards the sediment-water interface, is more pronounced at STA04 compared to STA10 ($\delta^{56}Fe_{pw}$ ~-2.4‰ vs. -0.9‰, respectively). Fe_{pw} becomes isotopically heavier with depth ($\delta^{56}Fe_{pw}$ increases) at STA04, but remains at ~-1.4‰ in the lower part of the ferruginous zone. Reliable $\delta^{56}Fe_{pw}$ data could not be produced further downcore due to low Fe_{pw} concentrations and low pore water recovery. $\delta^{56}Fe_{pw}$ at STA10 is more variable at depth: from 2 to ~15 cm, covering the Fe^{2+} maximum, it varies between -0.9 and -0.5‰. Between 14 and 18 cm there is a slight trend towards lower $\delta^{56}Fe_{pw}$ values, followed by an increase to near zero values at ~30 cm depth. The shift towards most negative $\delta^{56}Fe_{pw}$ values (-1‰) occurs 25 cm below the maximum Fe^{2+} concentrations.

There is a correlation of $\delta^{56}Fe_{pw}$ with $\delta^{56}Fe_{aca}$ with r^2 = 0.86 at STA10 when two depths (16 and 18 cm) are eliminated from the calculation (Fig. 6a). Fe_{aca} is isotopically light compared to Fe_{pw} in the top 9 cm of the sediment, whereas below, Fe_{aca} is isotopically heavier (Fig. 6b).

Similar to Fe_{pw}, Fe_{aca} is isotopically light at STA04 (-0.5 to -1‰) and STA10 (-0.25 to -1‰) (Fig. 5a, c). $\delta^{56}Fe_{hyam}$ deviates from the typical terrestrial background value of ~0.09‰ (Beard et al. 2003) with -1.04‰ to -0.19 at STA04 (trend towards more positive values at depth) and -0.23‰ ± 0.18‰ at STA10 (error is 2SD). In contrast, Fe_{di-ct} and Fe_{oxa} do not show pronounced fractionation. There is only a slight overall enrichment in ^{56}Fe in the Fe_{di-ct} pool: $\delta^{56}Fe_{di-ct}$ is 0.26 ± 0.13‰ at STA04 and 0.16 ± 0.16‰ at STA10 (Fig. 5a, c). $\delta^{56}Fe_{oxa}$ values are 0.11 ± 0.13‰ and 0.06 ± 0.16‰, respectively.

5   Discussion

5.1   Spatial differences in early diagenesis

Sediments show a strong variability in the thickness of the ferruginous zone and the shape of sulfate profiles at the sites in Potter Cove and Maxwell Bay. There is a tendency to broad ferruginous zones and only slight increases of dissolved compounds related to organic matter degradation (alkalinity, ammonia) with depth at stations proximal to glacier fronts (Fig. 3c). In contrast, sediments in deep troughs in the central bay and especially sites, where oxic surface meltwater streams discharge, show rather condensed redox zones: There, sulfate concentrations decrease and alkalinity and ammonia increase significantly with depth (Fig. 3a, b). The subsurface Fe^{2+} maxima indicate that at all investigated sites Fe is actively used as an electron acceptor for the decomposition of organic matter. Minor depletion of sulfate concentrations (except for STA13) at stations close to the glacier terminus (Group III) indicates that in these sediments Fe is a more important electron acceptor than SO_4^{2-}.

Total organic carbon (TOC) contents are low (<0.5 wt%, Monien et al. 2014) in surface sediments in the eastern part of Potter Cove that has been ice-covered until a few decades ago (Rückamp et al. 2011). The contents vary between 0.5 and 1.3 wt% in the southern, central, and

northwestern part of Potter Cove (Monien et al. 2014). Organic matter mainly derives from local macro-algae that are abundant in hard bottom areas of the outer cove, but sparse in the eastern part and close to the glacier front (Quartino and Boraso de Zaixso 2008, Quartino et al. 2013, Monien et al. 2014). Freshwater algae have been observed in surface streams of KGI (e.g., Lee et al. 2009) and may represent an additional, but minor organic matter source for marine sediments in the bay. Higher accumulation rates of detrital material in the eastern compared to the western part of Potter Cove might dilute the TOC content and lower the availability of degradable organic matter even further. However, variable TOC contents fail to explain the observed differences in redox zonation between sites STA04 and STA10 that as they are both located in the organic matter-lean eastern part of Potter Cove.

Sediment accumulation rates in Potter Cove were estimated by Monien et al. (2017) based on ^{210}Pb dating of three sediment cores. Two of the cores were from the eastern part of Potter Cove and revealed a strong increase in sediment accumulation since 1940, when the glacier developed from a grounded to a tidewater glacier. Sediment accumulation was <0.15 g cm^{-2} yr^{-1} before and 0.15-0.45 g cm^{-2} yr^{-1} after 1940. Average sediment accumulation rates over the past 20 years are 0.33 ± 0.14 g cm^{-2} yr^{-1}. Sediment accumulation calculated from sediment trap data resulted in slightly higher rates and showed that high sedimentation events occur as a result of an increase of water discharge by meltwater streams draining the eastern ice-free area of Potter Peninsula (Monien et al. 2017). In order to cause the observed differences in the redox zonation, accumulation rates (determining the transport of electron acceptors into the sediment) would have to be considerably higher at STA10 compared to STA04. Average sediment accumulation rates at STA04 and STA10 are, however, assumed to be similar based on the findings by Monien et al. (2017). It is noteworthy that the two cores in the eastern part of Potter Cove that were investigated by Monien et al. (2017) could be dated back until 1870 although according to Rückamp et al. (2011) this area has been ice-covered until at least 1956. We conclude that the depositional evolution of Potter Cove is not sufficiently understood. In general, sediment deposition and erosion in Potter Cove show a strong dependency

on topography and bed shear stresses (Wölfl et al. 2014). Therefore, we assume that the thickness of the sediment cover over hard ground can vary significantly over short distances. Based on the data by Rückamp et al. (2011) STA10 is ice-free since about the early 1960s, STA04 since about the 1980s. It is probable that the different depositional regimes at these stations and the different timing of exposure from glacial ice results in different thicknesses of the sediment cover.

In the northeastern Potter Cove at the glacier front, the content of easily reducible Fe (oxyhydr)oxides is particularly high (Fe_{hyam} at STA10: 0.28 ± 0.03 wt%, ~15% of Fe_{react}, Fig. 5a) compared to sediments in the south (Fe_{hyam} at STA04: 0.18 ± 0.03 wt%, ~8.5% of Fe_{react}, Fig. 5c). Vandieken et al. (2006) observed concurring DIR and sulfate reduction in the top 2 cm of fjord sediments of NE-Svalbard in the Arctic, which confirmed the finding by Jakobsen and Postma (1994), Postma and Jakobsen (1996), Jørgensen and Kasten (2006), and Canfield and Thamdrup et al. (2009) that in natural sediments DIR and sulfate reduction zones often overlap or occur in reverse order. However, when amorphous Fe oxides are present, Fe reduction is favored over sulfate reduction (Postma and Jakobsen 1996). We suggest that the high availability of easily reducible Fe oxides results in or at least contributes to a broader ferruginous zone in the sediments close to the glacier front of Potter Cove. A similar pattern was observed in sediments from Kongsfjorden and Van Keulenfjorden in Western Svalbard with a comparative glacial margin configuration (Wehrmann et al. 2014).

The linear decrease in pore water sulfate concentrations with depth at STA10 suggests that only minor net consumption of sulfate occurs within the sampled sediments. The shape of profile at STA04, in contrast, implies that sulfate is drawn down to a sulfate-methane transition (SMT) located at about 55 cm sediment depth, where it is consumed by the anaerobic oxidation of methane (AOM) (e.g., Niewöhner et al. 1998, Adler et al. 2000). Similarly shallow depths of the SMT have been observed in temperate and subpolar shelf sediments (e.g., Oni et al. 2015, Geprägs et al. 2016). The linear sulfate profile at STA10 can potentially be explained by a thinner sediment cover compared to STA04. If the sediments are not thick enough to favour methane formation, there is no AOM and

consequently no SMT that would result in a decrease of SO_4^{2-} with depth. Unfortunately, we do not have information about the sediment thicknesses within Potter Cove or at our sampling locations.

Besides the combined availability of organic matter and easily reactive Fe oxides, physical reworking of sediment is known to increase microbial Mn- and Fe-reduction because it replenishes solid Fe- and Mn-phases by back-oxidation of liberated Mn^{2+} and Fe^{2+} (e.g., Aller et al. 1986, Canfield 1989). Physical reworking likely plays an important role in bays with marine-terminating or tidewater glaciers such as Potter Cove, where intense ice-scouring, especially close to glacier fronts, occurs. In particular STA10, located close to the glacier front, might be affected by ice-scouring. The general decrease of Fe_{react} as well as the presence of a trend in $\delta^{56}Fe_{aca}$ over depth at STA10 points against a complete mixing of the sediment column. We therefore consider reworking processes as a possible additional, but not the only reason for organic matter degradation being largely driven by Fe reduction.

All of the above mentioned factors are dependent on the position of the glacier terminus relative to the shore. This suggests that the retreat of glaciers and (in the extreme case) the transition of a marine- to a land-terminating glacier is accompanied by significant changes of sediment and reducible Fe input, which affects the distribution of benthic habitats (Jerosch et al. 2018) and is thus worthy of investigation. Our data imply that the availability of highly reactive Fe (oxyhydr)oxides (Fe_{hyam}), as the parameter that shows strong differences between STA04 and STA10, as well as the thickness of the sediment cover allowing or not allowing methane generation at depth play important roles in determining the early diagenetic reactions in Potter Cove. We did not have the possibility to investigate the latter issue, but consider it valuable to identify the factors that ultimately regulate highly reactive Fe contents in Potter Cove as these might also impact diagenetic pathways in similar settings elsewhere. Thus, we must consider the processes by which highly reactive Fe can be supplied to sediments from glaciated margins in the first instance.

5.2   Sources of easily reducible Fe (oxyhydr)oxides in glaciomarine sediments

Easily reducible Fe oxides can derive from terrestrial sources, oxidation and precipitation of Fe in the water column and from precipitation of upward diffusing Fe_{pw} at the sedimentary oxic/suboxic redox boundary (e.g., Kasten et al. 1998, Haese 2000). Glaciers may represent additional sources of easily reducible Fe (oxyhydr)oxides: They provide large quantities of eroded bedrock and may, through biogeochemical weathering, also produce dissolved Fe^{2+} and secondary Fe nanoparticles at the glacier bed (e.g., Bhatia et al. 2013, Wadham et al. 2013). The reactivity of these Fe phases at the time of their introduction into the coastal and marine environment depends on the reaction pathways during their transport. 1) When glaciers terminate on land, the surficial (oxic) meltwater streams transport physically eroded silicates and Fe-oxides as well as secondary (nano)particulate Fe (oxyhydr)oxides. Dissolved Fe is largely oxidized on its way to the coast and most of the suspended matter is typically deposited in the estuary (Fig. 2; Statham et al. 2008, Bhatia et al. 2013, Hawkings et al. 2014, Zhang et al. 2015, Hodson et al. 2017). 2) Marine-terminating glaciers provide basically similar reactive Fe phases, but as subglacial water is directly injected into the marine water, the export of reactive Fe phases (Fe nanoparticles and dissolved Fe) into the marine system is presumably more efficient compared to land-terminating glaciers (Fig. 2). In addition, marine-terminating glaciers produce icebergs that are known to contain reactive Fe nanoparticles and are considered important for the long-distance transport of Fe from the Antarctic coast into the SO (Raiswell et al. 2006, 2016, Hopwood et al. 2017). 3) Groundwater (also fed by (sub)glacial meltwater) can also deliver substantial amounts of aqueous Fe^{2+}/Fe^{3+} and nanoparticulate Fe (oxyhydr)oxides, especially if there is submarine discharge and water is still anoxic upon injection into the marine environment (e.g., Wadham et al. 2013). An interplay between pyrite oxidation and DIR was postulated by Dold et al. (2013) to result in groundwater Fe^{2+} plumes that discharge into the coastal ocean of Marian Cove located north of Potter Cove (Fig. 1). Submarine groundwater discharge was also directly observed at high rates at the marginal ice zone of East

Antarctica (Uemura et al. 2011). In the following we elucidate which Fe transport and reaction pathways are potentially important in Potter Cove and Maxwell Bay.

5.2.1 Land-terminating glacial meltwater runoff

Dissolved Fe concentration data of surficial (oxic) meltwater streams at King George Island are not available. However, dissolved or filterable Fe concentrations (defined differently as <0.2, <0.4 or <0.45 µm) from glacial outflow in other glaciated environments range between 20 and 9950 nM (Statham et al. 2008, Bhatia et al. 2013, Hawkings et al. 2014, Zhang et al. 2015, Hodson et al. 2017). Dissolved Fe concentrations in glacial runoff at Livingston Island bordering Maxwell Bay to the Southwest was found to be 1350 ± 1125 nM and about twice as high as non-glacial runoff (Hodson et al. 2017). Zhang et al. (2015) showed that surface meltwater streams might be more significant sources of particulate than of dissolved Fe into the ocean, because ~98% of the dissolved Fe is lost by precipitation during the route through the proglacial terrain and the estuary (also see Boyle et al. 1977).

Suspended matter (SPM) loads of surficial meltwater streams that discharge into Potter Cove vary by several orders of magnitude between different stream systems and sampling dates (Monien et al. 2017). Based on SPM contents of the four major surface meltwater tributaries of Potter Peninsula into Potter Cove and their discharge volumes, Monien et al. (2017) calculated a SPM discharge of 3×10^3 t per year into Potter Cove. The authors estimated that 85% of the SPM that is introduced via meltwater streams are deposited within Potter Cove. SPM from surficial meltwater streams draining Potter Peninsula was shown to be slightly weathered and to contain significantly less ascorbate-leachable (bioavailable) Fe (0.03 wt%) than Potter Cove surface sediments (0.11 wt%) (Monien et al. 2017). Consistent with this, we exclude surficial oxic meltwater streams as the predominant source of easily reducible Fe oxides, because easily reducible Fe contents were higher (absolute and relative) at STA10 (glacier front) compared to STA04 (discharge of surficial meltwater).

5.2.2   Subglacial runoff from marine-terminating glaciers and submarine groundwater discharge

Monien et al. (2017) determined the vertical sediment flux in Potter Cove based on sediment trap data and found that the amount of sediment that accumulates is an order of magnitude higher than what is delivered by surficial oxic meltwater streams. The authors concluded that a sediment amount of 20 to 36 x 10^3 t yr^{-1} directly derives from subglacial sources and suggested a massive discharge of subglacial water carrying high contents of fine-grained, potentially reactive Fe-rich particles. Bedrock beneath glaciers is efficiently comminuted by glacial physical erosion. The resultant glacial flour may then be transported into the coastal ocean by subglacial meltwater or by iceberg rafting.

Our data show that glacially eroded bedrock is also a source of pyrite for Potter Cove sediments: This is indicated by significantly higher FeS_2 contents at STA10 compared to the STA04 (Fig. 5b, d) even though sulfate reduction is more apparent at the latter site. A decrease of pore water Fe^{2+} below the Fe^{2+} maximum produced by DIR usually indicates the reaction front with H_2S and the formation of Fe sulfides (e.g., Canfield 1989, Oni et al. 2015, Riedinger et al. 2017). Even at STA10, where the sulfate profile shows rather constant values throughout the core (Fig. 4f), such a Fe^{2+} sink is indicated at 25 cm depth (10 cm at STA04). Ongoing sulfidization is further suggested by a general decrease of the Fe oxide content (Fig. 4e) and an increase of S/Al ratios and Fe_{pyrite} with depth (Figs. 4e, 5d). However, pyrite is present at both stations throughout the cores including the surface sediment. Sediments are potentially affected by iceberg scraping at STA10 and bioturbation was observed at STA04. These processes could lead to a transport of diagenetically formed pyrite to the sediment/water interface. However, Dold et al. (2013) estimated the pyrite content in rocks of KGI to be ~2.6 wt%. Glacially (physically) eroded pyrite would accumulate close to its source as it is a heavy mineral. Therefore, it is likely that particularly STA10 receives pyrite from comminuted bedrock, transported into the bay via subglacial meltwater. Dissolved Fe resulting from biogeochemical weathering at the glacier bed may be transported directly into the ocean via subglacial drainage pathways. Such direct anoxic meltwater discharge may represent a so far underestimated Fe source (Wadham et al. 2013). Dold et al. (2013) observed Fe^{2+}-rich groundwater

outflow from beneath the Fourcade Glacier in Marian Cove that is adjacent to Potter Cove. Alongside the study by Monien et al. (2017) that indicates massive subglacial discharge of Fe-rich rock flour into Potter Cove, it can be assumed that a subglacial drainage system beneath Fourcade Glacier is a key source of dissolved and particulate Fe. Subglacial drainage pathways are characterized by a high rock-water contact and water residence times that may cause a development into anoxic conditions and a release of Fe from fine-grained particles into solution.

Sulfide oxidation is a dominant biogeochemical weathering process beneath glaciers (e.g., Tranter et al. 2002, Statham et al. 2008, Skidmore et al. 2010, Wadham et al. 2010). Subglacial environments are known to sustain a wide variety of oxic and anoxic microbial habitats as fine-grained material provides ample contact surfaces (Sharp et al. 1999, Skidmore et al. 2000, 2005, Mikucki et al. 2004, 2009). Sulfide oxidation can fuel silicate weathering (by providing protons for silicate hydrolysis) and microbial iron reduction (by providing Fe (oxyhydr)oxides if it takes place under oxic conditions) (e.g., Wadham et al. 2010). When the system develops towards anoxia, sulfide oxidation proceeds through the reduction of ferric Fe (e.g., Williamson and Rimstidt et al. 1994, Nordstrom and Southam 1997, Holmes and Crundwell 2000, Tranter et al. 2002, Jørgensen et al. 2009), in which case aqueous Fe^{2+} is liberated. This process continues as long as Fe^{3+} is available, so it requires a back-reaction of Fe^{2+} to Fe^{3+}. Aqueous Fe (Fe^{2+}/Fe^{3+}) produced by chemical weathering and microbial activity in subglacial environments can either accumulate in the meltwaters and then be discharged into the coastal ocean or be recycled within the system, which presumably enhances the variability of its isotopic composition (Stevenson et al., 2017). Dold et al. (2013) suggested that pyrite oxidation and the resulting acid rock drainage are major sources of dissolved Fe in Antarctic groundwater. We also consider this process as one of the main contributors to dissolved Fe in subglacial waters beneath the Fourcade Glacier.

It is likely that a large part of the Fe delivered by direct discharge of subglacial water and groundwater is retained in shelf sediments due to fast oxidation and precipitation in the proximal water column (Fig. 2; Boyle et al. 1977, Wadham et al. 2013).

5.3 Indication of iron sources by sedimentary stable iron isotopes

Processes leading to subglacial Fe^{2+}/Fe^{3+} liberation are likely to be microbially mediated (Tranter et al. 2002, Mikucki et al. 2009, Lanoil et al. 2009, Skidmore et al. 2010, Wadham et al. 2010, Dold et al. 2013, Boyd et al. 2014) and are thus assumed to preferentially release ^{54}Fe. Subglacial discharge should thus be characterized by low δ^{56}Fe values of dissolved Fe compared to the source rock if DIR or other microbially mediated redox reactions are the predominant Fe liberation processes. Stable Fe isotope data with respect to subglacial outflows is very limited. Recently, Stevenson et al. (2017) showed that depending on the degree of chemical weathering in the subglacial environment subglacial discharge from the Greenland ice sheet represent a source of isotopically light Fe (down to -2.1‰). Dissolved Fe from Blood Falls draining Taylor Glacier in East Antarctica had δ^{56}Fe values of -2.6‰ (Mikucki et al. 2009). While Stevenson et al. (2017) linked the fractionation of Fe isotopes to silicate weathering and sulfide oxidation, the light isotopic composition of dissolved Fe in the Blood Falls was related to microbial redox cycling and DIR beneath Taylor Glacier.

Precipitation of amorphous Fe oxyhydroxides from isotopically light outflows could explain the overall light isotopic signal of easily reducible Fe (Fe_{hyam}) at STA10. The form of Fe at the time of entrance into the seawater (aqueous Fe^{2+}, Fe^{3+} or solid Fe(III)) cannot be discriminated with the data produced in our study. However, isotopically light Fe inputs in form of dissolved or amorphous Fe oxyhydroxides into Potter Cove would imply that the residual source material (fine-grained bedrock) that undergoes biogeochemical alteration becomes enriched in ^{56}Fe. The slightly positive δ^{56}Fe values of the less reactive Fe fractions Fe_{di-ct} and Fe_{oxa} at STA04 and STA10 might be indicative for that although we cannot resolve how much of this heavier isotope signal must be attributed to *in situ* Fe reduction. Further work is needed to compare sequentially extracted SPM from turbid meltwater plumes with the isotopic composition of the sediments. It is noteworthy that isotope fractionation also occurs during the oxidation and precipitation of aqueous Fe^{2+} to Fe^{3+} or solid Fe(III) (e.g., Bullen et al. 2001, Welch et al. 2003, Balci et al. 2006, Staubwasser et al. 2013). However, these

fractionations cannot be resolved here. Fe^{2+}, Fe^{3+} and solid Fe(III) are considered as one pool that (in sum) is isotopically light compared to the original bedrock Fe.

It is a valid assumption that pyrite oxidation affects the chemical composition of melt- and groundwater discharged into Potter Cove. The site in Marian Cove, where pyrite oxidation and acid rock drainage was observed (Dold et al. 2013), is only about 3 km away from STA10. At that location, the beach in front of the glacier was accessible and discharge of Fe^{2+}-rich ground water was observed just above the high tide level. In the northeastern part of Potter Cove, the calving front of the tidewater glacier could not be sampled for safety reasons. Marian and Potter Cove are divided by Barton Peninsula. It appears unlikely that there are striking differences in the biogeochemical processes occurring at the rock-glacier interface at the northern side of Barton Peninsula (Marian Cove) compared to the southern side (Potter Cove). Furthermore, acidophilic chemolithoautotrophic bacteria that use Fe(III) as electron acceptors have been found at the nearby Cardozo Cove (~10 km from Potter Cove), which is also affected by acid rock drainage (Dold et al. 2013). Such low pH fluids mix with seawater, Fe^{2+} oxidises and precipitates, forming nanoparticulate Fe (oxyhydr)oxides. Accordingly, Dold et al. (2013) observed abundant jarosite, goethite, schwertmannite, and ferrihydrite at Marian Cove, where the latter appeared to form closest to the seawater front. Schwertmannite typically forms at pH 2-5 and ferrihydrite at neutral pH (Bigham et al. 1996). Both minerals transform into goethite and hematite (e.g., Schwertmann and Carlson 2005, Davidson et al. 2008) whereby the half-life of ferrihydrite at low temperatures as they prevail in Antarctic waters is in the order of years (Cornell and Schwertmann 2003, Raiswell 2011, Raiswell and Canfield 2012). We assume that a large part of the Fe delivered by subglacial (anoxic) meltwaters in Potter Cove is retained in shelf sediments close to the glacier front due to fast oxidation and precipitation in the water column. Flocculation may, however, promote a lateral transport of particles (Schroth et al. 2014, Markussen et al. 2016) as it was observed for 15% of the SPM in Potter Cove that is exported into Bransfield Strait (Monien et al. 2017).

5.3.1 In-situ isotope fractionation vs. fingerprint of subglacial discharge

In the following discussion we focus on Fe_{pw}, Fe_{aca}, and Fe_{hyam} as those are considered the reactive pools in terms of early diagenetic Fe cycling. In principle, Fe_{aca} comprises surface-adsorbed Fe(II) ($Fe(II)_{sorb}$) and Fe dissolved from AVS and carbonates if present (Table 1). Based on analysis of North Sea sediments, Henkel et al. (2016) found that $Fe(II)_{sorb}$ may dominate Fe_{aca} in natural sediments. $\delta^{56}Fe_{aca}$ may track the Fe isotopic composition of ambient Fe_{pw} as the isotopic composition of $Fe(II)_{sorb}$ lies between that of Fe_{pw} and solid Fe(III) (e.g., Williams and Scherer 2004, Crosby et al. 2007). Fractionation factors ($\Delta Fe_{A-B} = \delta^{56}Fe_A - \delta^{56}Fe_B$) between aqueous Fe ($Fe_{aq}$) and $Fe(II)_{sorb}$ are estimated to be ~-0.9‰ (Crosby et al. 2005, 2007) or -1.24‰ (Beard et al. 2010) where fractionation is most pronounced during the initial state of DIR and becomes less distinct when the reaction continues for a longer period of time. Fractionation factors at equilibrium are ~-0.8‰ for Fe_{aq} and $Fe(II)_{sorb}$ ($\Delta Fe_{Feaq-Fe(II)sorb}$) (Wu et al. 2011), ~-0.49‰ for $\Delta Fe_{Fe(II)sorb-hematite}$ (Wu et al. 2009), -1.2‰ for $\Delta Fe_{Fe(II)sorb-goethite}$ (Beard et al. 2010), and -2.58 to -3.17‰ for $\Delta Fe_{Feaq-HFO}$ (Wu et al. 2011), where HFO are hydrous ferric oxides. From these values it can be concluded that (when in equilibrium) the easily reducible Fe (oxyhydr)oxides would be ~1.7 to 2.3‰ heavier than $Fe(II)_{sorb}$ (Fe_{aca} pool). Fresh, isotopically light Fe_{AVS} that potentially also contributes to Fe_{aca} would further increase the isotopic difference between Fe_{aca} and Fe_{hyam}. The discrepancy between the isotopic composition of Fe_{aca} and Fe_{hyam} is, however, much smaller at the investigated sites (0.4 ± 0.3‰), which indicates that a comparatively small fraction of the available highly reactive Fe oxides underwent microbial reduction and/or that the fractionation is dominated by kinetic effects rather than equilibrium exchange, which is not unlikely in natural open systems.

At STA10, the linear correlation between $\delta^{56}Fe_{aca}$ and $\delta^{56}Fe_{pw}$ (Fig. 6a) indicates that there is a process affecting the isotopic composition of both pools. The slight trend to more positive $\delta^{56}Fe$ values with depth of both, Fe_{pw} and Fe_{aca} (Figs. 4f, 5c, and 6b), is in agreement with a progressive depletion of the ^{54}Fe pool during ongoing early diagenetic cycling (see below). However, the relationship between Fe_{pw} and Fe_{aca} is not straight-forward. Extractions with acetate may liberate

AVS-Fe (Poulton and Canfield 2005). Fe_{AVS}/Fe_{aca} ratios are shown in Fig. 5b and d. They indicate that in some layers, especially at STA10 and the deeper samples of STA04, up to 60% of Fe_{aca} may derive from Fe monosulfides. Thus, the potential effect of Fe_{AVS} on the isotopic composition of Fe_{aca} has to be taken into account. Fe_{aca} in the top 9 cm of the sediment (STA10) is isotopically light compared to Fe_{pw} ($\delta^{56}Fe_{aca}$ = -0.90 ± 0.08‰, n = 7; $\delta^{56}Fe_{pw}$ = -0.73 ± 0.07‰, n = 8; Fig. 6b). This could be explained by kinetically controlled FeS precipitation (dominating in natural environments over equilibrium fractionation): Freshly formed FeS is isotopically light compared to ambient pore water with $\Delta^{56}Fe_{Feaq-FeS}$ = 0.85 ± 0.30‰ (Butler et al. 2005). Equilibrium Fe isotope fractionation would show an opposite trend, i.e. an enrichment of ^{56}Fe in FeS compared to Fe_{pw} (Guilbaud et al. 2011). Below 15 cm, Fe_{aca} is consistently heavier than Fe_{pw}, which might indicate a change of the process leading to isotope fractionation or changing relative proportions of carbonate-bound Fe, Fe_{AVS}, and $Fe(II)_{sorb}$ contributing to the isotopic composition of Fe_{aca}. This explanation is supported by a strong variability of Fe_{aca}/Fe_{react} over depth (Fig. 5c), strongly varying contributions of Fe_{AVS} to Fe_{aca} (Fig. 5d) and an overall good correlation between Fe_{aca}/Fe_{react} and $\delta^{56}Fe_{aca}$ (r^2 = 0.54).

The easily reducible Fe oxide fraction (Fe_{hyam}) shows negative $\delta^{56}Fe$ values over the whole core length at both sites (Fig. 5). A depletion in ^{56}Fe of such a reactive phase in marine sediments is generally interpreted as involvement in *in situ* early diagenetic Fe cycling (e.g., Staubwasser et al. 2006, Homoky et al. 2009, Henkel et al. 2016). When fractionation due to early diagenesis occurs, the largest depletion in ^{56}Fe is typically observed at the top of the sediment column as there, redox cycling is most intense. ^{56}Fe becomes enriched in the ferric substrate with increasing sediment depth during ongoing DIR, balancing out the isotopically light Fe^{2+} that is liberated (e.g., Staubwasser et al. 2006, Crosby et al. 2007). $\delta^{56}Fe_{pw}$ follows the trend towards more positive values with depth because $^{54}Fe(III)$ becomes less available. Overall, the trends in $\delta^{56}Fe_{pw}$ and $\delta^{56}Fe_{hyam}$ at STA04 are typical for such *in situ* Fe fractionation by early diagenetic redox cycling. In contrast, there is no trend towards heavier $\delta^{56}Fe_{hyam}$ values with depth at STA10. A complete and frequent mixing of the whole sediment column, e.g. by ice-scouring, seems unlikely as there are trends with depth in $\delta^{56}Fe_{aca}$ (Fig. 5c). Fe_{hyam} must have undergone *in situ* redox cycling to some extent because we observed a broad ferruginous

zone with Fe^{2+} values of up to 100 µM. $\delta^{56}Fe_{pw}$ values at STA10 are rather constant around -0.7‰ in the top 10 cm ($\delta^{56}Fe_{hyam} \approx$ -0.25‰). The Fe isotopic composition of pore water is affected by Fe sulfide formation below 25 cm depth, which is indicated by modestly heavier $\delta^{56}Fe_{pw}$ values and the drawdown in Fe^{2+} concentrations that typically indicates a balancing with or outbalancing by H_2S. The fact that despite pronounced DIR $\delta^{56}Fe_{pw}$ and $\delta^{56}Fe_{hyam}$ are so constant suggests that the Fe_{hyam} pool is overwhelmingly large in relation to what is actually reduced by microorganisms. Due to the larger Fe substrate pool at STA10, microorganisms will theoretically encounter and reduce the isotopically heavier substrate less frequently than they would at STA04. Not even the precipitation of secondary Fe (oxyhydr)oxides in the oxic zone of the sediment is quantitatively important enough to leave an imprint in the $\delta^{56}Fe$ composition of the highly reactive Fe pool that we could analytically resolve.

Considering that STA10 (i) might obtain reactive Fe from direct subglacial discharges (as discussed above) due to its location and that (ii) subglacial chemical alteration of minerals is partly driven by microbes (e.g., Singer et al. 1970, Kimura et al. 2011) and thus likely results in Fe isotope fractionation, we suggest that the Fe_{hyam} pool already exhibited a light $\delta^{56}Fe$ composition at the time of deposition in Potter Cove sediments. The isotopic composition of Fe_{di-ct} and Fe_{oxa} at STA10 does not considerably deviate from the average igneous rock value suggesting that these pools are mainly of detrital origin or that only a small fraction of these crystalline phases was affected by biogeochemical weathering driving their $\delta^{56}Fe$ values slightly towards positive values. The original isotopic composition of Fe_{hyam} and, thus, the contribution of subglacial material to sediments at STA04 cannot be assessed based on the data presented here, because of the early diagenetic overprint. We suggest that there is a significant input of isotopically light Fe in form of aqueous Fe^{2+}, Fe^{3+} or secondary Fe nanoparticles in the vicinity of the glacier, which likely results from direct discharge of potentially anoxic subglacial waters or groundwater.

5.3.2   Variability of pore water $\delta^{56}Fe$ and iron fluxes

The δ^{56}Fe signature of dissolved Fe in the water column is considered a potential tool to detect and quantify benthic Fe fluxes (e.g., Conway and John 2014). This appears to be a very elegant approach, but it requires comprehensive knowledge about the regional variability of the processes that determine δ^{56}Fe$_{pw}$. With this study we provide a basis to assess whether or not δ^{56}Fe signatures of dissolved Fe can be used for benthic flux estimates from shelf sediments in polar bays.

Since largest Fe isotope fractionation is commonly observed during DIR, one could assume that sediments in Potter Cove (all affected by DIR) are characterized by distinct δ^{56}Fe values, especially where the reactive Fe pool is the main driver of organic matter degradation. STA10 showed DIR but no net sulfate reduction, which results in overall negative δ^{56}Fe values of Fe$_{pw}$ and highly reactive Fe pools. Most negative δ^{56}Fe values were, however, obtained at shallow depth at the STA04, where the ferruginous zone is comparatively narrow and where sulfate reduction is indicated by sulfide smell and the linear decrease of sulfate concentrations with depth. The pattern can be explained by mass balance, where the isotopic difference between two pools, e.g., ferric substrate and Fe$_{pw}$, is determined by the relative size of the pools. Severmann et al. (2010) demonstrated a wide spatio-temporal variability of the reductive end-member of δ^{56}Fe$_{pw}$ in shelf sediments across the shelf along Oregon–California. In agreement to this, we consider that even when focusing on one bay such as Potter Cove, a quantification of benthic fluxes based on water column δ^{56}Fe will be challenging as there is not a defined endmember value for δ^{56}Fe$_{pw}$ at the sediment-water interface. The values at different sites can be assumed to vary by several per mill. Benthic flux estimates therefore require stable isotope mass-balance models that consider uncertainties in endmember signatures as used by Conway and John (2014).

Monien et al. (2014) estimated Fe fluxes across the sediment-water interface in Potter Cove using gradients of measured pore water Fe profiles. These fluxes varied between 1.4 and 155 mmol m^{-2} yr^{-1} and were comparable to those in Svalbard fjord sediments in (Wehrmann et al. 2014). The overall distribution pattern of sedimentary redox zones in Potter Cove indicates steeper Fe^{2+} gradients at sites with characterized by net sulfate reduction compared to DIR-dominated sites.

Steeper gradients imply that more Fe^{2+} might reach the sediment/water interface or ultimately escape into the water column. If glacier retreat goes along with a development of DIR-dominated sites due to increased input of highly reactive Fe, this does consequently not necessarily go along with an increase benthic Fe fluxes.

The distinction of subglacial discharge from benthic fluxes is complicated by the overlapping nature of the Fe isotopic signals and their variability which is insufficiently explored. Such an approach would have to be complemented by the use of additional tracers such as $\delta^{18}O$ or radioisotopes and in-depth knowledge of hydrography and seasonality. The importance of such *a priori* knowledge with respect to the setup of isotope mass-balance models was also emphasized by Homoky et al. (2016).

We find evidence that subglacial meltwaters introduce isotopically light, easily reducible Fe (oxyhydr)oxides into Potter Cove sediments. Our study suggests that in combination with independent proxies $\delta^{56}Fe$ can represent a useful tool to detect subglacial meltwater discharge and could potentially be applied to investigate abiotic and microbially driven weathering processes at glacier beds.

6   Conclusions

The use of $\delta^{56}Fe$ for an identification and quantification of Fe fluxes in polar coastal and marine environments requires a much better understanding of the spatial and temporal variability of early diagenetic iron cycling in these areas than we have at present. Pore water profiles from 14 sites in fjords of King George Island showed that the degradation of organic matter in sediments close to marine-terminating glaciers is largely driven by DIR, whereas sites proximal to oxic surface meltwater streams and those in central parts of Potter Cove also show significant sulfate reduction. Two of these contrasting sites, STA10 at the marine terminus of the Fourcade Glacier and STA04 at the discharge of a surface meltwater stream, were chosen for $\delta^{56}Fe$ analyses of pore water and

sequentially leached Fe phases. The broad ferruginous zone at STA10 compared to STA04 can be related to higher absolute and relative contents of easily reducible Fe (oxyhydr)oxides and potentially the absence of methanic sediments and a sulfate-methane transition at depth. However, in general, the heterogeneous distribution of organic matter in Potter Cove sediments may also contribute to the observed large variability in pore water profiles. Although DIR seems to be a major pathway of organic matter degradation at STA10 close to the glacier front, we observed a larger variability in δ^{56}Fe, both in pore water and easily reducible Fe oxides, at STA04. The δ^{56}Fe signature of the highly reactive Fe phase (ferrihydrite, lepidocrocite) at STA10 was generally negative (-0.25‰) and rather constant within the ferruginous zone. DIR not going along with an imprint on the isotopic composition of pore water or the easily reducible Fe fraction indicates that the available pool of reactive Fe exceeds the need by iron reducers by far. Therefore, we interpret the overall negative δ^{56}Fe signature of the highly reactive Fe as "inherited" signal from iron redox cycling before this fraction actually deposited in Potter Cove. Previous studies indicated that subglacial meltwater discharge may be significant in the study area. Dold et al. (2013) found acid rock drainage related to subglacial pyrite oxidation at two bays of King George Island (Marian Cove north of Potter Cove and Cardozo Cove, part of Admiralty Bay, ~10 km north-east of Potter Cove) and Monien et al. (2017) proposed that a large part of SPM within the water column of Potter Cove is related to glacial physical weathering and rock flour exported in subglacial meltwaters. Highly reactive particulate Fe contents observed at STA10 and corresponding low δ^{56}Fe values of this fraction point toward a similar interpretation, as they can be explained by input of microbially recycled Fe from the subglacial environment beneath Fourcade Glacier. Resulting aqueous Fe (either Fe^{3+} or Fe^{2+}) could be transported by subglacial meltwater, oxidize in the water column or during transport and form highly reactive Fe (oxyhydr)oxides (mostly nanoparticulate ferrihydrite). The freshly formed amorphous Fe seems to accumulate close to the glacier front, where it fuels DIR.

The pore water isotopic composition at the investigated sites showed large variability with stronger fractionation close to the surface meltwater discharge compared to the site at the glacier

front. A quantification of benthic Fe fluxes and subglacial Fe discharges based on stable Fe isotope geochemistry will be complicated because (1) diagenetic processes vary strongly at short lateral distances and (2) the variability of δ^{56}Fe in subglacial meltwater has not been sufficiently well investigated yet. However, isotope mass balance models that consider the current uncertainties could, in combination with the application of ancillary proxies, lead to a much better quantification of Fe inputs into polar marine waters than currently available. This would consequently allow a better assessment of the flux and fate of Fe originating from the Antarctic Ice Sheet.

We observed the highly reducing and Fe isotope-fractionating nature of the glacial margin systems on the Antarctic Peninsula, which collectively appears able to impart a significantly light composition and high abundance of dissolved Fe into coastal waters. These signatures might be detectable in waters and sediment archives further offshore around the Antarctic continent.

MARUM project SD2 (Post-depositional cycling and fractionation of Fe in dependence on sediment dynamics and depositional regime). Data are available in the Pangaea database (https://doi.pangaea.de/10.1594/PANGAEA.890315).

References

Adler M. , Hensen C. , Kasten S. and Schulz H. D. (2000) Computer simulation of deep sulfate reduction in sediments of the Amazon Fan, *Int. Journ. Earth Sciences* **88**, 641-654.

Aller R. C., Mackin J. E. and Cox Jr. R. T. (1986) Diagenesis of Fe and S in Amazon inner shelf muds: apparent dominance of Fe reduction and implications for the genesis of ironstones. *Cont. Shelf Res.* **6**(1/2), 263-289.

Beard B. L., Johnson C. M., Skulan J. L., Nealson K. H., Cox L. and Sun H. (2003) Application of Fe isotopes to tracing the geochemical and biological cycling of Fe. *Chem. Geol.* **195**, 87–117.

Beard B. L. and Johnson C.M. (2004) Fe isotope variations in the modern and ancient Earth and other planetary bodies. *Rev. Mineral. Geochem.* **55**, 319-357.

Beard B. L., Handler R. M., Scherer M. M., Wu L., Czaja A. D., Heimann A. and Johnson C. M. (2010) Iron isotope fractionation between aqueous ferrous iron and goethite. *Earth Planet. Sci. Lett.* **295**, 241–250.

Bhatia M. P., Kujawinski E. B., Das S. B., Breier C. F., Henderson P. B. and Charette M. A. (2013) Greenland meltwater as a significant and potentially bioavailable source of iron to the ocean. *Nat. Geosci.* **6**, 274-278.

Bigham J. M., Schwertmann U., Traina S. J., Winland R. L. and Wolf M. (1996) Schwertmannite and the chemical modelling of iron in acid sulphate waters. *Geochim. Cosmochim. Acta* **60**, 2111-2121.

Boyd P. W. (2002) Environmental factors controlling phytoplankton processes in the Southern Ocean. *J. Phycol.* **38**, 844-861.

Boyd E. S., Hamilton T. L., Havig J. R., Skidmore M. L. and Shock E. L. (2014) Chemolithotrophic Primary Production in a Subglacial Ecosystem. *Appl. Environ. Microbiol.* **80**(19), 6146–6153.

Boyle E. A., Edmond J. M. and Sholkovitz E. R. (1977) Mechanism of iron removal in estuaries. *Geochim. Cosmochim. Acta* **41**(9), 1313–1324.

Bullen T. D., White A. F., Childs C. W., Vivit D. V. and Schulz M.S. (2001) Demonstration of significant abiotic iron isotope fractionation in nature. *Geology* **29**(8), 699–702.

Butler I. A., Archer C., Vance D., Oldroyd A. and Rickard D. (2005) Fe isotope fractionation on FeS formation in ambient aqueous solution. *Earth Planet. Sci. Lett.* **236**, 430– 442.

Canfield D. E. (1989) Reactive iron in marine sediments. *Geochim. Cosmochim. Acta* **53**, 619-632.

Canfield D. E., Raiswell R., Westrich J. T., Reaves C. M. and Berner R. A. (1986) The use of chromium reduction in the analysis of reduced inorganic sulfur in sediments and shales. *Chem. Geol.* **54**, 149–155.

Canfield D. E. and Thamdrup B. (2009) Towards a consistent classification scheme for geochemical environments, or, why we wish the term 'suboxic' would go away. *Geobiology* **7**, 385–392.

Conway T. M. and John S. G. (2014) Quantification of dissolved iron sources to the North Atlantic Ocean. *Nature* **511**, 212-215.

Cook A. J., Fox A. J., Vaughan D. G. and Ferrigno J. G. (2005) Retreating glacier fronts on the Antarctic Peninsula over the past half-century. *Science* **308**, 541-544.

Cornell R. M. and Schwertmann U. (2003) The iron oxides: structure, properties, reactions, occurrences and uses. Wiley, New York.

Cornwell J. C. and Morse J. W. (1987) The characterization of iron sulfide minerals in anoxic marine sediments. *Mar. Chem.* **22**, 193– 206.

Croot P. L. and Laan P. (2002) Continuous shipboard determination of Fe(II) in polar waters using flow injection analysis with chemiluminescence detection. *Anal. Chim. Acta* **466**(2), 261-273.

Crosby H. A., Johnson C. M., Roden E. E. and Beard B. L. (2005) Coupled Fe(II)–Fe(III) electron and atom exchange as a mechanism for Fe isotope fractionation during dissimilatory iron oxide reduction. *Environ. Sci. Technol.* **39**, 6698–6704.

Crosby H. A., Roden E. E., Johnson C. M. and Beard B. L. (2007) The mechanism of iron isotope fractionation produced during dissimilatory Fe(III) reduction by *Shewanella putrefaciens* and *Geobacter sulfurreducens*. *Geobiology* **5**, 169–189.

Davidson L. E., Shaw S., and Benning L. G. (2008) The kinetics and mechanisms of schwertmannite transformation to goethite and hematite under alkaline conditions. *Am. Mineral.* **93**, 1326-1337.

Death R., Wadham J. L., Monteiro F., Le Brocq A. M., Tranter M., Ridgwell A., Dutkiewicz S. and Raiswell R. (2014) Antarctic ice sheet fertilises the Southern Ocean. *Biogeosciences* **11**, 2635-2644.

De Jong J., Schoemann V., Lannuzel D., Croot P., de Baar H. and Tison J.-L. (2012) Natural iron fertilization of the Atlantic sector of the Southern Ocean by continental shelf sources of the Antarctic Peninsula. *J. Geophys. Res.* **117**, G01029.

Dierssen H. M., Smith R. C., and Vernet M. (2002) Glacial meltwater dynamics in coastal waters west of the Antarctic peninsula. *PNAS* **44**(9), 1790–1795.

Dold B., Gonzalez-Toril E., Aguilera A., Lopez-Pamo E., Cisternas M. E., Bucchi F. and Amils R. (2013) Acid Rock Drainage and Rock Weathering in Antarctica: Important sources for iron cycling in the Southern Ocean. *Environ. Sci. Technol.* **47**, 6129-6136.

Falk U., López D. A. and Silva-Busso A. (2018) Multi-year analysis of distributed glacier mass balance modelling and equilibrium line altitude on King George Island, Antarctic Peninsula. *TC* 12, 1211-1232.

Fantle M. S. and DePaolo D. J. (2004) Iron isotopic fractionation during continental weathering. *Earth Planet. Sci. Lett.* **228**, 547-562.

Ferguson D. (1921) Geological observations in the South Shetlands, the Palmer Archipelago, and Graham Land, Antarctica. *Trans. Roy. Soc. Edin.* **53** (1)(3), 29-55.

Geprägs P., Torres M.E., Mau S., Kasten S., Römer M., and Bohrmann G. (2016) Carbon cycling fed by methane seepage at the shallow Cumberland Bay, South Georgia, sub-Antarctic. *Geochem. Geophys. Geosyst.* **17**, 1401– 1418.

Guilbaud R., Butler I. B., Ellam R. M., Rickard D. and Oldroyd A. (2011) Experimental determination of the equilibrium Fe isotope fractionation between Fe^{2+}_{aq} and FeS_m (mackinawite) at 25 and 2°C. *Geochim. Cosmochim. Acta* **75**, 2721–2734.

Haese R. R., Schramm J., Rutgers van der Loeff M. M. and Schulz H.D. (2006) A comparative study of iron and manganese diagenesis in continental slope and deep sea basin sediments off Uruguay (SW Atlantic). *Int. Journ. Earth Sciences* **88**, 619–629.

Hawkings J. R., Wadham J. L., Tranter M., Raiswell R., Benning L. G., Statham P. J., Tedstone A., Nienow P., Lee K. and Telling J. (2014) Ice sheets as a significant source of highly reactive nanoparticulate iron to the oceans. *Nat. Commun.* **5:3929**, doi: 10.1038/ncomms4929.

Henkel S., Kasten S., Poulton S.W. and Staubwasser M. (2016) Determination of the stable iron isotopic composition of sequentially leached iron phases in marine sediments. *Chem. Geol.* **421**, 93– 102.

Hodson A., Nowak A., Sabacka M., Jungblut A., Navarro F., Pearce D., Ávila-Jiménez M. L., Convey P., and Vieira G. (2017) Climatically sensitive transfer of iron to maritime Antarctic ecosystems by surface runoff. *Nat. Commun.* **8**, 14499.

Holmes P. R. and Crundwell F. K. (2000) The kinetics of the oxidation of pyrite by ferric ions and dissolved oxygen: An electrochemical study. *Geochim. Cosmochim. Acta* **64**(2), 263–274.

Homoky W. B., Severmann S., Mills R. A., Statham P. J. and Fones G.R. (2009) Pore-fluid Fe isotopes reflect the extent of benthic Fe redox recycling: Evidence from continental shelf and deep-sea sediments. *Geology* **37**(8), 751–754.

Hopwood M. J., Statham P. J., Tranter M. and Wadham J. L. (2014) Glacial flours as a potential source of Fe(II) and Fe(III) to polar waters. *Biogeochemistry* **118**, 443–452.

Hopwood M. J., Cantoni C., Clarke J. S., Cozzi S. and Achterberg E.P. (2017) The heterogeneous nature of Fe delivery from melting icebergs. *Geochem. Persp. Let.* **3**, 200-209.

Jakobsen R. and Postma D. (1994) In situ rates of sulfate reduction in an aquifer (Rømø, Denmark) and implications for the reactivity of organic matter. *Geology* **23**, 1103-1106.

Jerosch K., Pehlke H., Monien P., Scharf F., Weber L., Kuhn G., Braun M. H. and Abele D. (2018) Benthic meltwater fjord habitats formed by rapid glacier recession on King George Island, Antarctica. *Phil. Trans. R. Soc. A* **376**: 20170178.

John S. G., Mendez J., Moffett J. and Adkins J. (2012) The flux of iron and iron isotopes from San Pedro Basin sediments. *Geochim. Cosmochim. Acta* **93**, 14-29.

Johnson C. M. and Beard B. L. (2005) Biogeochemical cycling of iron isotopes. *Science* **309**, 1025-1027.

Jørgensen C. J., Jacobsen O. S., Elberling B. and Aamand J. (2009) Microbial oxidation of pyrite coupled to nitrate reduction in anoxic groundwater sediment. *Environ. Sci. Technol.* **43**(13), 4851-4857.

Jørgensen B.B. and Kasten S. (2006) Sulfur Cycling and Methane Oxidation. In: Schulz H.D. and Zabel M. (eds.) Marine Geochemistry, Springer Berlin Heidelberg, p. 271-309.

Kimura S., Bryan C. G., Hallberg K. B. and Johnson D. B. (2011) Biodiversity and geochemistry of an extremely acidic, low-temperature subterranean environment sustained by chemolithothrophy. *Environ. Microbiol.* **13**(8), 2092–2104.

Kasten S., Freudenthal T., Gingele F. X. and Schulz H. D. (1998) Simultaneous formation of iron-rich layers at different redox boundaries in sediments of the Amazon Deep-Sea Fan, *Geochim. Cosmochim. Acta* **62**, 2253–2264.Klöser H., Ferreyra G., Schloss I., Mercuri G., Laturnus F., and Curtosi A. (1994) Hydrography of Potter Cove, a small fjord-like inlet on King George Island (South Shetlands). *Estuar. Coast. Shelf Sci.* **38**, 523–537.

Kraus S. and del Valle R. (2008): Geology, tectonics and Ar-Ar ages of the magmatic dykes from Potter Peninsula (King George Island, South Shetland Islands). In Wiencke C., Ferreyra G.A., Abele D. and Marenssi S., The Antarctic ecosystem of Potter Cove, King-George Island (Isla 25 de Mayo), Berichte zur Polar- und Meeresforschung, p. 20-30.

Lanoil B., Skidmore M., Priscu J. C., Han S., Foo W., Vogel S., Tulaczyk S. and Engelhardt H. (2009) Bacteria beneath the West Antarctic Ice Sheet, *Environ. Microbiol.* **11**(3), 609–615.

Lee Y. I., Lim H. S. and Yoon H.I. (2009) Carbon and nitrogen isotope composition of vegetation on King George Island, maritime Antarctic. *Polar Biol.* **32**, 1607–1615.

Littlefair M. J. (1978) The quartz-pyrite rock of South Shetland Islands, western Antarctic Peninsula. *Econ. Geol.* **73**(6), 1184-1189.

Lohan M. C., Aguilar-Islas A. M., Franks R. P. and Bruland K.W. (2005) Determination of iron and copper in seawater at pH 1.7 with a new commercially available chelating resin, NTA Superflow. *Anal. Chim. Acta* **530**, 121–129.

Lovley D. R. (1991) Dissimilatory Fe(III) and Mn(IV) Reduction. *Microbiol. Rev.* **55**(2), 259-287.

Markussen T. N., Elberling B., Winter C. and Andersen T. J. (2016) Flocculated meltwater particles control Arctic land-sea fluxes of labile iron. Scientific Reports **6**, 24033.

Martin J. H. (1990) Glacial-interglacial CO_2 change: The iron hypothesis. *Paleoceanography* **5**(1), 1-13.

Mikucki J. A., Foreman C. M., Sattler B., Lyons W. B. and Priscu J. C. (2004) Geomicrobiology of Blood Falls: an iron-rich saline discharge at the terminus of the Taylor Glacier, Antarctica. *Aquat. Geochem.* **10**(3-4), 199-220.

Mikucki J. A., Pearson A., Johnston D. T., Turchyn A. V., Farquhar J., Schrag D. P., Anbar A. D., Priscu J. C. and Lee P.A. (2009) A contemporary microbially maintained subglacial ferrous "ocean". *Science* **324**, 397-400.

Mikucki J. A., Lee P. A., Ghosh D., Purcell A. M., Mitchell A. C., Mankoff K. D., Fisher A. T., Tulaczyk S., Carter S., Siegfried M. R., Fricker H. A., Hodson T., Coenen J., Powell R., Scherer R., Vick-Majors T., Achberger A. A., Christner B. C., Tranter M. and the WISSARD Science Team (2016) Subglacial Lake Whillans microbial biogeochemistry: a synthesis of current knowledge. *Phil. Trans. R. Soc.* A **374**, 20140290.

Monien D., Monien P., Brünjes R. M., Silva-Busso A., Schnetger B., Widmer T., Kappenberg A. and Brumsack H.-J. (2017) Meltwater as a source of potentially bioavailable iron to Antarctic waters. *Antarct. Sci.* **29**(3), 277-291.

Monien P., Lettmann K. A., Monien D., Asendorf S., Wölfl A.-C., Lim C. H., Thal J., Schnetger B. and Brumsack H.-J. (2014) Redox conditions and trace metal cycling in coastal sediments from the maritime Antarctic. *Geochim. Cosmochim. Acta* **141**, 26-44.

Niewöhner C., Hensen C., Kasten S., Zabel M. and Schulz H. D. (1998) Deep sulfate reduction completely mediated by anaerobic methane oxidation in sediments of the upwelling area off Namibia, *Geochim. Cosmochim. Acta* **62**, 455–464.

Nixon S. L., Telling J. P., Wadham J. L. and Cockell C. S. (2017) Viable cold-tolerant iron-reducing microorganisms in geographically diverse subglacial environments. *Biogeosciences* **14**, 1445–1455.

Nordstrom D. K. and Southam G. (1997) Geomicrobiology of sulfide mineral oxidation. In: Banfield J.F. and Nealson K.H. (eds.) Geomicrobiology: Interactions between Microbes and Minerals. Mineralogical Society of America, Washington, pp. 361-390.

Oni O., Miyatake T., Kasten S., Richter-Heitmann T., Fischer D., Wagenknecht L., Kulkarni A., Blumers M., Shylin S. I., Ksenofontov V., Costa B. F. O., Klingelhöfer G. and Friedrich M. W. (2015) Distinct microbial populations are tightly linked to the profile of dissolved iron in the methanic sediments of the Helgoland mud area, North Sea. *Front. Microbiol.* **6:365**, doi: 10.3389/fmicb.2015.00365.

Postma D. and Jakobsen R. (1996) Redox zonation: Equilibrium constraints on the Fe(III)/SO$_4$-reduction interface. *Geochim. Cosmochim. Acta* **60**(17), 3169-3175.

Poulton S. W. (2003) Sulfide oxidation and iron dissolution kinetics during the reaction of dissolved sulfide with ferrihydrite. *Chem. Geol.* **202**, 79–94.

Poulton S. W., Krom M. D. and Raiswell R. (2004) A revised scheme for the reactivity of iron (oxyhydr)oxide minerals towards dissolved sulfide. *Geochim. Cosmochim. Acta* **68**, 3703-3715.

Poulton S. W. and Canfield D. E. (2005) Development of a sequential extraction procedure for iron: implications for iron partitioning in continentally derived particulates. *Chem. Geol.* **214**, 209–221.

Quartino M. L. and Boraso de Zaixso A. L. (2008) Summer macroalgal biomass in Potter Cove, South Shetland Islands, Antarctica: its production and flux to the ecosystem. *Polar Biol.* **31**, 281-294.

Quartino M. L., Deregibus D., Campana G. L., Latorre G. E. J. and Momo F. R. (2013) Evidence of macroalgal colonization on newly ice-free areas following glacial retreat in Potter Cove (South Shetland Islands), Antarctica. *PLoS One* **8**, e58223.

Raiswell R. and Canfield D. E. (2012) The Iron Geochemical Past and Present. *Geochem. Perspect.* **1**(1).

Raiswell R. (2011) Iceberg-hosted nanoparticulate Fe in the Southern Ocean: Mineralogy, origin, dissolution kinetics and source of bioavailable Fe. *Deep Sea Res. II* **58**, 1364–1375.

Raiswell R., Tranter M., Benning L. G., Siegert M., Death R., Huybrechts P. and Payne T. (2006), Contributions from glacially derived sediment to the global iron (oxyhydr)oxide cycle: Implications for iron delivery to the oceans. *Geochim. Cosmochim. Acta* **70**, 2765– 2780.

Raiswell R., Benning L. G., Tranter M. and Tulaczyk S. (2008) Bioavailable iron in the Southern Ocean: the significance of the iceberg conveyor belt. *Geochem. Trans.* **9**(7), doi: 10.1186/1467-4866-9-7.

Raiswell R., Hawkings J. R., Benning L. G., Baker A. R., Death R., Albani S., Mahowald N., Krom M. D., Poulton S. W. and Wadham J. (2016) Potentially bioavailable iron delivery by iceberg-hosted sediments and atmospheric dust to the polar oceans. *Biogeosciences* **13**, 3887-3900.

Riedinger N., Brunner B., Krastel S., Arnold G. L., Wehrmann L. M., Formolo M. J., Beck A., Bates S. M., Henkel S., Kasten S. and Lyons T. W. (2017) Sulfur cycling in an iron oxide-dominated, dynamic marine depositional system: The Argentine continental margin. *Front. Earth Sci.* **5:33**, doi: 10.3389/feart.2017.00033.

Roese M. and Drabble M. (1998) Wind driven circulation in Potter Cove. In: Wiencke C., Ferreyra G. A., Arntz W. and Rinaldi C. (eds) The Potter Cove Coastal Ecosystem, Antarctica. *Reports on Polar Research* **299**. Karl Kamloth, Bremen, pp. 40–46.

Rouxel O. J. and Auro M. (2010) Iron isotope variations in coastal seawater determined by Multicollector ICP-MS. *Geostand. Geoanal. Res.* **34**(2), 135-144.

Rückamp M., Blindow N., Suckro S., Braun M. and Humbert A. (2010) Dynamics of the ice cap on King George Island, Antarctica: Field measurements and numerical simulations. *Ann. Glaciol.* **51**(55).

Rückamp M., Braun M., Suckro S. and Blindow N. (2011) Observed glacial changes on the King George Island ice cap, Antarctica, in the last decade. *Glob. Planet. Change* **79**, 99–109.

Sarazin G., Michard G. and Prevot F. (1999) A rapid and accurate spectroscopic method for alkalinity measurements in sea water samples. *Water Res.* **33**(1), 290-294.

Schoenberg R. and von Blanckenburg F. (2005) An assessment of the accuracy of stable Fe isotope ratio measurements on samples with organic and inorganic matrices by high-resolution multicollector ICP-MS. *Int. J. Mass Spectrom*. **242**, 257–272.

Schöne T., Pohl M., Zakrajsek A. and Schenke H. (1998) Tide gauge measurements, a contribution for the long term monitoring of sea level. In: Wiencke C., Ferreyra G.A., Arntz W. and Rinaldi C. (eds) The Potter Cove Coastal Ecosystem, Antarctica. Reports on Polar Research 299. Karl Kamloth, Bremen, pp. 12–14.

Schroth A. W., Crusius J., Hoyer I. and Campbell R. (2014) Estuarine removal of glacial iron and implications for iron fluxes to the ocean. *Geophys. Res. Lett.* **41**, 3951-3958.

Schwertmann U. and Carlson L. (2005) The pH-dependent transformation of schwertmannite to goethite at 25 °C. *Clay Miner.* **40**, 63–66.

Seeberg-Elverfeldt J., Schlüter M., Feseker T. and Kölling M. (2005), Rhizon sampling of porewaters near the sediment-water interface of aquatic systems. *Limnol. Oceanogr. Methods* **3**, 361–371.

Severmann S., Johnson C. M., Beard B. L. and McManus J. (2006) The effect of early diagenesis on the Fe isotope compositions of porewaters and authigenic minerals in continental margin sediments. *Geochim. Cosmochim. Acta* **70**, 2006–2022.

Severmann S., McManus J., Berelson W. M., and Hammond D. E. (2010) The continental shelf benthic iron flux and its isotope composition. *Geochim. Cosmochim. Acta* **74**, 3984-4004.

Sharp M., Parkes J., Cragg B., Fairchild I. J., Lamb H. and Tranter M. (1999) Widespread bacterial populations at glacier beds and their relationship to rock weathering and carbon cycling. *Geology* **27**(2), 107–110.

Singer P. C. and Stumm W. (1970) Acidic Mine Drainage: The Rate-Determining Step. *Science* **167**, 1121-1123.

Skidmore M. L., Foght J. M. and Sharp M. J. (2000) Microbial Life beneath a High Arctic Glacier. *Appl. Environ. Microbiol.* **66**(8), 3214–3220.

Skidmore M., Anderson S. P., Sharp M., Foght J. and Lanoil B. D. (2005) Comparison of microbial community compositions of two subglacial environments reveals a possible role for microbes in chemical weathering processes. *Appl. Environ. Microbiol.* **71**(11), 6986–6997.

Skidmore M., Tranter M., Tulaczyk S. and Lanoil B. (2010) Hydrochemistry of ice stream beds—evaporitic or microbial effects? *Hydrol. Process.* **24**, 517–523.

So C. S., Yun S. T. and Park M. E. (1995) Geochemistry of a fossil hydrothermal system at Barton Peninsula, King George Island. *Antarct*. Sci. **7**, 63-72.

Statham P. J., Skidmore M. and Tranter M. (2008) Inputs of glacially derived dissolved and colloidal iron to the coastal ocean and implications for primary productivity. *Global Biogeochem. Cycles* **22**, GB3013, doi: 10.1029/2007GB003106.

Staubwasser M., v. Blanckenburg F. and Schoenberg R. (2006) Iron isotopes in the early marine diagenetic iron cycle. *Geology* **34**, 629–632.

Staubwasser M., Schoenberg R., von Blanckenburg F., Krüger S. and Pohl C. (2013). Isotope fractionation between dissolved and suspended particulate Fe in the oxic and anoxic water column of the Baltic Sea. *Biogeoscience*s **10**, 233–245.

Stevenson E., Fantle M. S., Das S. B., Williams H. M. and Aciego S. M. (2017) The iron isotopic composition of subglacial streams draining the Greenland ice sheet. *Geochim. Cosmochim. Acta* **213**, 237-254.

Stookey L. L. (1970) Ferrozine – A new spectrophotometric reagent for iron. *Analytical Chemistry* **42**(7), 779 –781.

Tranter M., Sharp M. J., Lamb H. R., Brown G. H., Hubbard B. P. and Willis I. C. (2002) Geochemical weathering at the bed of Haut Glacier d'Arolla, Switzerland—a new model. *Hydrol. Process.* **16**, 959-993.

Uemura T., Taniguchi M. and Shibuya K. (2011) Submarine groundwater discharge in Lützow-Holm Bay, Antarctica. *Geophys. Res. Lett.* **38**, L08402, doi:10.1029/2010GL046394.

Vandieken V., Finke N. and Jørgensen B. B. (2006) Pathways of carbon oxidation in an Arctic fjord sediment (Svalbard) and isolation of psychrophilic and psychrotolerant Fe(III)-reducing bacteria. *MEPS* **322**, 29-41.

Wadham J. L., Tranter M., Skidmore M., Hodson A. J., Priscu J., Lyons W. B., Sharp M., Wynn P. and Jackson M. (2010) Biogeochemical weathering under ice: Size matters. *Global Biogeochem. Cycles* **24**, GB3025, doi:10.1029/2009GB003688.

Wadham J. L., Arndt S., Tulaczyk S., Stibal M., Tranter M., Telling J., Lis G. P., Lawson E., Ridgwell A., Dubnick A., Sharp M. J., Anesio A. M. and Butler C. E. H. (2012) Potential methane reservoirs beneath Antarctica. *Nature* **488**, 633-637.

Wadham J., Death R., Monteiro F. M., Tranter M., Ridgwell A., Raiswell R. and Tulaczyk S. (2013) The potential role of the Antarctic Ice Sheet in global biogeochemical cycles. *Earth Environ. Sci. Trans. R. Soc. Edinburgh* **104**, 55–67.

Wehrmann L. M., Formolo M. J., Owens J. D., Raiswell R., Ferdelman T. G., Riedinger N. and Lyons T. W. (2014) Iron and manganese speciation and cycling in glacially influenced high-latitude fjord sediments (West Spitsbergen, Svalbard): Evidence for a benthic recycling-transport mechanism. *Geochim. Cosmochim. Acta* **141**, 628–655.

Welch S. A., Beard B. L., Johnson C. M. and Braterman P. S. (2003) Kinetic and equilibrium Fe isotope fractionation between aqueous Fe(II) and Fe(III). *Geochim. Cosmochim. Acta* **22**, 4231-4250.

Williams A. G. B. and Scherer M. M. (2004) Spectroscopic evidence for Fe(II)-Fe(III) electron transfer at the iron oxide-water interface. *Environ. Sci. Technol.* **38**, 4782-4790.

Williamson M. A. and Rimstidt J.D. (1994) The kinetics and electrochemical rate-determining step of aqueous pyrite oxidation. *Geochim. Cosmochim. Acta* **58**(24), 5443-5454.

Wölfl A.-C., Lim C. H., Hass H. C., Lindhorst S., Tosonotto G., Lettmann K.A., Kuhn G., Wolff J.-O. and Abele D. (2014) Distribution and characteristics of marine habitats in a subpolar bay based on hydroacoustics and bed shear stress estimates - Potter Cove, King George Island, Antarctica. *Geo-Mar. Lett*. **34**(5), 435-446.

Wu L., Beard B. L., Roden E. E. and Johnson C. M. (2009) Influence of pH and dissolved Si on Fe isotope fractionation during dissimilatory microbial reduction of hematite. *Geochim. Cosmochim. Acta* **73**(19), 5584–5599.

Wu L., Beard B. L., Roden E. E. and Johnson C. M. (2011) Stable iron isotope fractionation between aqueous Fe(II) and hydrous ferric oxide, *Environ. Sci. Technol*. **45**, 1847–1852.

Zhabina N. N. and Volkov I. I. (1978) A method of determination of various sulphur compounds in sea sediments and rocks. In: Krumbein W. E. (ed.), Environmental biogeochemistry: Methods, metals and assessment, Volume 3. Ann Arbor Science Publishers (Michigan), 735-746.

Zhang R., John S. G., Zhang J., Ren J., Wu Y., Zhu Z., Liu S., Zhu X., Marsay C. M. and Wenger F. (2015) Transport and reaction of iron and iron stable isotopes in glacial meltwaters on Svalbard near Kongsfjorden: From rivers to estuary to ocean. *Earth Planet. Sci. Lett.* **242**, 201-211.

Figure captions

Figure 1:   Study area in the west of King George Island and close-up of Potter Cove (PC) showing the sites of sediment sampling in 2012 and 2013. Bathymetric data derive from Arndt et al. (2013). Ice cover is represented by white areas. Marian Cove and Collins Harbour are indicated as MC and CH, respectively. (Map generated by K. Jerosch)

Figure 2:   Schematic drawing showing different iron transport and reaction pathways from the glacier to the coastal sea and into marine sediments. The close-up illustrates the early diagenetic redox cycling of Fe in the sediment. Fe^{2+} and Fe^{3+} denote the dissolved, Fe(III) the solid Fe pool. Sediment cores from Potter Cove were classified into Group I, II, and III with regard to their relative location to the glacier terminus and the discharge of surficial meltwater streams as depicted here.

Figure 3:   Pore water profiles of stations from Potter Cove and Maxwell Bay are grouped according to their environmental characteristics. Sediments affected by meltwater discharge and those that accumulated in troughs of Potter Cove generally show more condensed redox zones compared to those that are close to glacier fronts.

Figure 4:   Geochemical data of STA04 including a) sequentially leached Fe fractions, b) Fe_{total} and Fe_{react}, Fe_{total}/Al, Fe_{react}/Fe_{total}, Mn/Al and S/Al, c) pore water SO_4^{2-}, Fe^{2+} and $\delta^{56}Fe_{pw}$ and respective geochemical data of STA10 (d-f)Solid phase and pore water data were gained for parallel cores. Error bars for SO_4^{2-} and Fe^{2+} are smaller than the symbol size.

Figure 5:   Sequentially extracted Fe fractions normalized to reactive Fe and respective $\delta^{56}Fe$ for STA04 (a) and STA10 (c). The solid grey lines indicate average values. Dashed grey lines indicate 2SD. AVS- and pyrite-Fe for STA04 (b) and STA10 (d) are given in wt%.

Note that AVS-Fe can form part of the Fe_{aca} fraction as acetate dissolves Fe monosulfides. Therefore, the ratio Fe_{AVS}/Fe_{aca} is give as dashed line.

Figure 6: $\delta^{56}Fe_{pw}$ vs. $\delta^{56}Fe_{aca}$ of STA10 (a) indicates a linear correlation between the two fractions with depth. Thus both fractions are affected by early diagenetic cycling. However, the link is not straightforward. In the top 10 cm of the sediment, Fe_{aca} is isotopically light compared to Fe_{pw} ($Fe_{pw} - Fe_{aca}$ = 0.07 to 0.30‰), whereas below, Fe_{aca} tends to be is isotopically heavier than Fe_{pw} with a maximum fractionation of -0.57‰ at 18 cm depth, where AVS-Fe contents are highest (b).

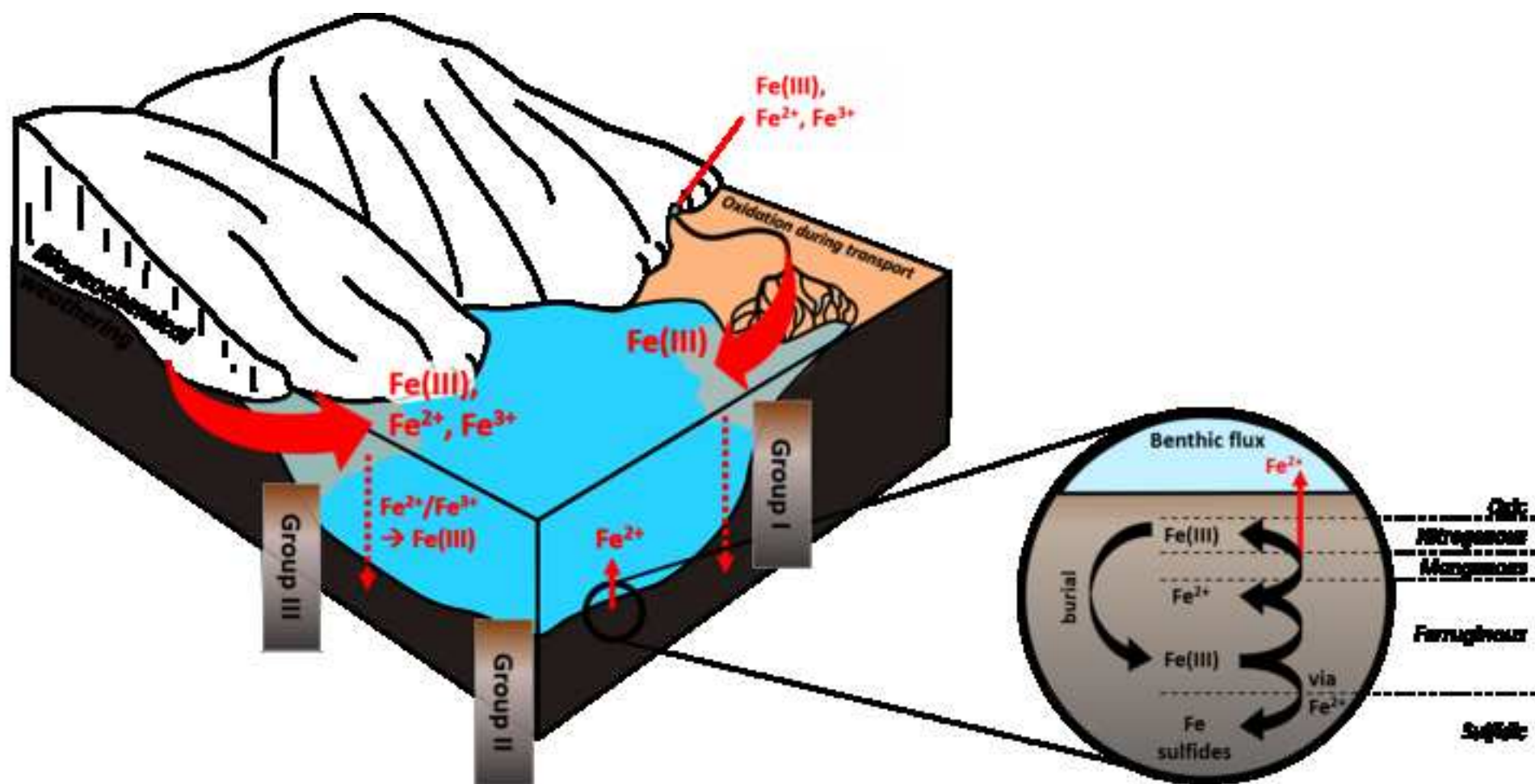**Table captions**

Table 1: List of parameters and respective abbreviations.

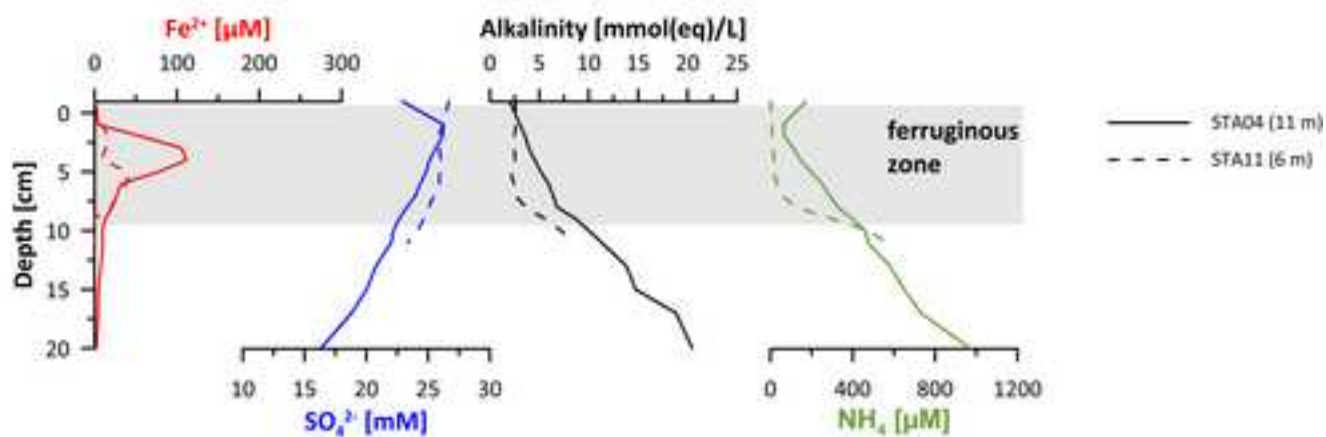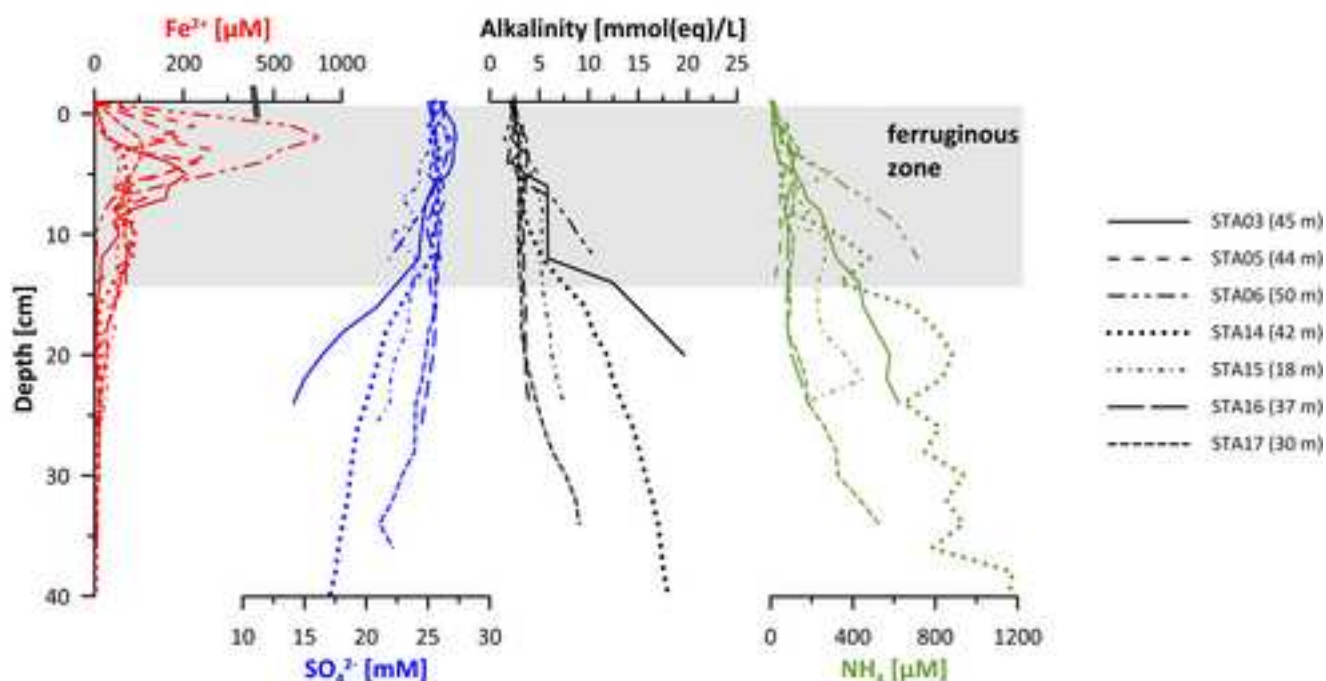| Abbreviation	Parameter
AVS	Acid volatile sulfur
CRS	Chromium reducible sulfur
DIR	Dissimilatory iron reduction
Fe_{AVS}	Fe bound in monosulfides (calculated from AVS content)
Fe_{pyrite}	Fe bound in pyrite (calculated from CRS content)
Fe_{aca}	Na-acetate leachable Fe fraction; carbonate-bound Fe, surface-adsorbed (or surface-reduced)Fe(II)
Fe_{hyam}	Hydroxylamine-HCl leachable Fe; easily reducible Fe-oxides (ferrihydrite, lepidocrocite)
Fe_{di-ct}	Na-dithionite leachable Fe; reducible Fe-oxides (mostly goethite and hematite)
Fe_{oxa}	Ammonium oxalate/oxalic acid leachable Fe; magnetite
Fe_{total}	Total sedimentary Fe content
Fe_{react}	Reactive Fe (sum of Fe_{aca}, Fe_{hyam}, Fe_{di-ct}, and Fe_{oxa})
$Fe(II)_{sorb}$	Surface-adsorbed Fe(II)
$\delta^{56}Fe_{pw}$	$\delta^{56}Fe$ of pore water; Note that Fe_{pw} is the total 'dissolved' Fe (not only Fe^{2+}).
Fe_{aq}	Aquatic Fe; used for discussion of experimentally determined fractionation factors
HFO	Hydrous ferric oxides
SPM	Suspended matter
TOC	Total organic carbon
TN	Total nitrogen

a) y = 2.133x + 0.612
r² = 0.86